

Microkinetic Modeling of Propane dehydrogenation (PDH)

On Pt-based catalyst

&

Thermal Cracking of Propane: Parameter estimation

A Project Report

Submitted in partial fulfillment of the
requirements for the degree of

Master of Technology

in the faculty of Engineering

by

Khomveer Singh

Under the guidance of

Prof. S. Venugopal & Prof. C.S. Laxinarasimhan



Department of Chemical Engineering

Indian Institute of Science

Bangalore 560012 (India)

June 2021

TABLE OF CONTENTS

CHAPTER 1: Microkinetic modeling of Propane dehydrogenation (PDH) on Pt-based catalyst

1. Introduction	1
2. Microkinetic modeling	4
2.1 Formulation of a microkinetic model	5
2.1.1 Formulation of a reaction mechanism	5
2.1.2 Thermodynamic consistency	5
2.1.3 Rate constant estimation	6
2.1.4 Microkinetic model development	7
3. Literature Survey	8
3.1 Adsorption of propane and propylene	8
3.2 Propane dehydrogenation to form propylene	9
3.3 Deep dehydrogenation	10
3.3.1 Dehydrogenation of propylene and formation of propylene	10
3.3.2 C-C cracking of C ₃ intermediates	11
4. Statement of the problem	12
4.1 Reaction scheme proposed for PDH on Pt catalyst	12
4.2 Modeling of reactions	19
4.2.1 Formulation of rate laws	19
4.2.2 Microkinetic and reactor model	20
4.3 Data collection from the work of Siddiqi et. al.	22
4.3.1 Inlet molar flow rate for propane and hydrogen	23
4.3.2 Calculation of n_{Pt}	23
4.3.3 Site time yield (STY)	23
4.3.4 Conversion	24
4.4 Solution of differential algebraic equations (DAE) in Athena Visual Studio: Methodology	24
5. Results and discussion	25
6. Future work	28
7. References	29

CHAPTER 2: Thermal cracking of propane: parameter estimation

1. Problem statement	39
2. Modeling reactions	40
3. Data collection	40
4. Selection of basis and calculation of initial feed composition	41
5. Parameter estimation using Athena Visual Studio and Python Lmfit package	42
6. Results and discussion	42
7. References	45

CHAPTER 1

1. Introduction

Propylene is an important raw material for producing a wide variety of products such as polypropylene, acrylonitrile, acetone, cumene, oxo-alcohols, propylene oxide, etc. Conventional propylene production processes involve fluid catalytic cracking and steam cracking of naphtha and light diesel. However, due to the increasing demand for propylene and emergence of shale gas, there is a need for other technologies. In the past few years, increasing technologies for propylene production have been widely developed, such as propane dehydrogenation (PDH), the methanol-to-olefins (MTO) process, and the Fischer–Tropsch-to-olefins process. The propane dehydrogenation (PDH) offers an option to capture the marginal, additional capacity needed to meet propylene demand. Shale gas condensates can be used to produce propane, making the feedstock less expensive and abundant. Several PDH technologies such as Catofin, Oleflex, PDH, etc., are being used commercially. A brief comparison of these PDH technologies is given in Table 1^[1,2]. Dow Chemical estimated in 2016 estimated that the demand for propylene would grow at an average yearly pace of 2% to 3% by 2035.^[3]

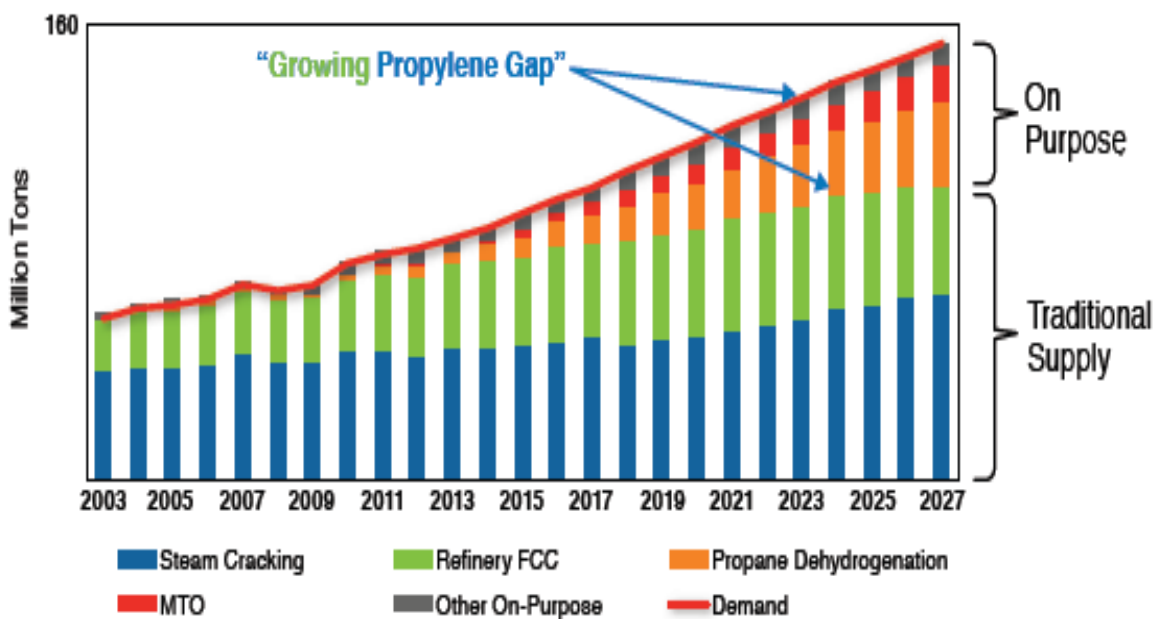
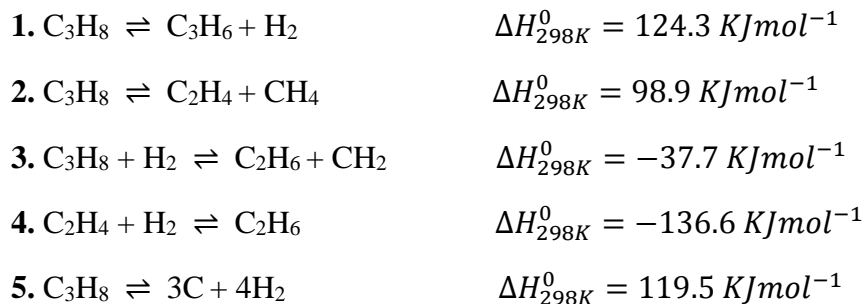


Figure 1: Various propylene production technologies and the supply-demand relationship of propylene^[3].

In PDH, propane gets converted into propylene and hydrogen on the surface of a catalyst, as illustrated below:



The reaction (1) is highly endothermic. Given stoichiometry of the reaction and enthalpy, increasing reaction temperature and decreasing pressure lead to higher propane conversions. Typical reaction conditions of PDH are 550-750 °C at pressure 1 bar^[4]. This reaction's drawback is equilibrium conversion and the presence of side reactions (2,3,4,5) at higher temperatures, thus decreasing propylene selectivity and deactivating the catalyst surface.

In the past several decades, a number of heterogeneous catalysts, including metal-based catalysts, metal oxide-based catalysts (such as Pt, CrO_x, VO_x, GaO_x)^[4,5] have been studied for direct PDH reaction due to their affinity for paraffinic C–H bonds and low activity to C–C cleavage that have exhibited high performances. However, the high tendency of coking, sintering, and cost requires further improved catalysts via unique preparation methods, support, and promoter.

Table 1: Summary of the catalytic data of representative propane dehydrogenation reaction technologies^[5]

Technology/ Licensor	CATOFIN (CB&I-ABB Lummus)	OLEFLEX (UOP LLC)	STAR (Krupp-Uhde)
Reactor type	Horizontal fixed bed reactor in a parallel arrangement	Vertical moving bed reactor in a series arrangement	Tubular fixed bed reactor
Catalyst	Chromium based CrO _x / Al ₂ O ₃	Platinum based Pt-Sn / Al ₂ O ₃	Pt-Sn / ZnAl ₂ O ₄ / CaO-Al ₂ O ₃
Reaction operating Condition (Temperature and Pressure)	560-650 °C 0.2-0.5 bar	525-705 °C 1-3 bar	560-650 °C 0.2-0.5 bar
Conversion	40-45 %	30-40 %	~35 %
Selectivity	80-90 %	85-90 %	80-90 %

Several processes for propane dehydrogenation have been emerged (as given in Table 1). Oleflex and Catofin processes have been industrialized and widely applied^[1,2], where Pt-based and CrOx-based catalysts have been commercialized, respectively. In the Catofin process, CrOx-based catalysts have been utilized due to their high catalytic activity and low price. However, besides their high environmental toxicity, the severe side reactions induce their quick deactivation and require frequent regeneration.^[9-11] Developing other metal oxide catalysts with low or non-chromium content is highly desired. Though the Pt catalyst shows excellent propane dehydrogenation activity due to its affinity for paraffinic C–H bonds and environmental friendliness^[4,5,11], its tendency to coking, sintering, and high cost still requires the development of low Pt-content and stable Pt-based. The difficulties mainly arise from the structural complexity of supported nanoparticles and the uncertainty of relevant preparation processes.^[5] Therefore, the exploitation of new efficient strategies for improving the stability of Pt-based and CrOx-based catalysts and finding alternative catalysts remain significant challenges.

It is generally accepted that numerous metal-based and metal oxide-based catalysts show superior activity and selectivity and have been widely developed. Still, it is unclear which active site structures and dehydrogenation mechanisms are followed in the PDH process from a fundamental perspective. Hence, it is vital to understand the relationship between active-site motifs and unique catalytic behaviors in the propane dehydrogenation system, including dehydrogenation pathways and deactivation mechanisms, which can shine a light on precise catalyst design.^[5]

The exact reaction mechanisms in the PDH process remain unclear. The complex nature of PDH and side reactions (deactivation and Cracking reactions) requires fundamental insight into the reaction mechanism, which gives a new direction to enhance catalyst design. A molecular-level understanding of such complex reaction networks can be achieved through the combined use of Computational chemistry (DFT, UBI-QEP, etc.) and Microkinetic modeling (MKM).

2. Microkinetic modeling

The design of heterogeneous catalysts relies on understanding the fundamental surface kinetics that controls catalyst performance, and microkinetic modeling is a tool that can help the researcher in streamlining the process of catalyst design^[6]. Microkinetic modeling identifies critical reaction intermediates, rate-determining elementary reactions, and dominant reaction paths, providing vital information for designing an improved catalyst and understanding reaction mechanisms at a more fundamental level.

Catalysis is mainly a kinetic phenomenon, and chemical kinetics is an essential tool in catalysis research. Reaction kinetics data are used in reactor design to study reaction mechanisms and elucidate a catalyst's structure–property relationship. The kinetics of a chemical reaction can be expressed as a power–law expression by regressing experimental data or by the LHHW (Langmuir–Hinshelwood–Hougen–Watson) rate expressions. Power law rate expression is a limiting approximation of a more complex rate expression. Thus, the apparent activation energy and the reaction orders obtained by regression of experimental data are valid for a limited range of reaction conditions. Additionally, little fundamental insight regarding the reaction mechanism can be obtained from simple power–law expressions. However, due to their simplicity and ease of use, the power-law rate expressions are appropriate for incorporating heat and mass transfer effects and, in some cases, catalyst deactivation^[31] in reactor design equations. As such, power-law rate expressions are widely used to operate industrial reactors.^[32,33] The LHHW rate expression for a reaction mechanism is obtained by assuming specific rate-determining elementary reactions, quasi-equilibrated elementary reactions, and the presence of most abundant surface intermediates (MASI). The LHHW rate expression is valid for a more comprehensive range of reaction conditions as compared to the power–law rate expression; however, the assumptions of Langmuir adsorption are implicit. Specifically, the LHHW rate expression assumes that all active sites for adsorption and reaction are identical and that interactions between adsorbed species are negligible. LHHW rate expressions are extensively used to model the performance of industrial reactors.^[34,35,36]

The traditional method outlined above provides valuable information, and researchers have used the data from these models coupled with chemical intuition to understand the reaction mechanism and design better catalysts. In this respect, obtaining information regarding the fundamental surface chemistry occurring on the catalyst surface is highly desirable as it accelerates and streamlines the process of rational catalyst design.

Microkinetic modeling breaks down a reaction mechanism into all known elementary steps making no a priori assumptions about dominant reaction paths, rate-determining steps, and most abundant reactive intermediates (MARI). Instead, this information emerges from the model's solution, and the effects of operating conditions on the reaction mechanism can also be determined.^[6]

2.1 Formulation of a microkinetic model

2.1.1 Formulation of a Reaction Mechanism

Catalytic processes proceed through combinations of elementary reactions. A sequence of elementary reactions based on the species' chemistry is postulated as the overall reaction mechanism. In general, a reaction mechanism includes adsorption of reactants, surface reaction, and desorption of products. However, a reaction mechanism can be complicated depending on the level of mechanistic detail that is included. The level of mechanistic details included in the reaction mechanism relies on the goal of the model^[6]. The complete reaction mechanism exhibits enormous complexity with hundreds of species and elementary reactions; however, this detailed mechanism is not necessary for most applications as only a few intermediates and elementary reactions are significant. Therefore, it is the choice of the researcher to include or exclude details based on experimental or computational evidence.

Significant research efforts in developing plausible reaction mechanisms have been undertaken, and various approaches for developing reaction mechanisms, particularly for complex systems, have been developed. These efforts include iterative methods,^[37] application of machine learning techniques,^[38,39] and reaction mechanism generating software programs like NetGen (Broadbelt and Klein)^[40], MECHEM (Valdés-Pérez)^[41], RING (Daoutidis and Bhan)^[42], and RMG-Cat (West and Green)^[43].

One possible solution to mitigate the increase in the number of intermediates and elementary reactions is to truncate the number of expansions with specific heuristics or rules,^[44] however, such an approach runs the risk of missing reactions that might be kinetically significant.^[45] Thus, the central challenge is to balance the need to include all elementary steps and the resources available for the estimation of kinetic parameters to determine kinetically relevant elementary reactions.

2.1.2 Thermodynamic consistency

Equilibrium constants for the i^{th} elementary reaction are calculated from Gibbs free energy changes, ΔG_i^0 of the i^{th} elementary step as:

$$K_{eq,i} = \exp\left(-\frac{\Delta G_i^0}{R^*T}\right) = \exp\left(\frac{\Delta S_i^0}{R}\right) * \exp\left(-\frac{\Delta H_i^0}{R^*T}\right) \quad (1)$$

Where $K_{eq,i}$ is the equilibrium constant of the i^{th} elementary reaction. ΔH_i^0 and ΔS_i^0 are the standard enthalpy and entropy change of the i^{th} elementary reaction, respectively. The enthalpy and entropy changes are obtained from experimental data or estimated by ab initio density functional theory

(DFT) calculations, the unity bond index-quadratic exponential potential (UBI-QEP) method, or scaling relations.

For any i^{th} elementary reaction, the ratio of forward rate ($k_{f,i}$) constant and backward rate constant ($k_{b,i}$) must be equal to the equilibrium of that elementary step as calculated from eq 1 i.e.

$$K_{eq,i} = \frac{k_{f,i}}{k_{b,i}} \quad (2)$$

2.1.3 Rate constant estimation

Rate constants for each elementary reaction are required to obtain the reaction rate. Generally, the rate constants are estimated using transition state theory or collision theory.

Collision theory: Rate constants for the adsorption and desorption of reactants and products can be estimated with collision theory. For the elementary adsorption reaction,



$$r_A = \sigma(T) * f(\theta_r) * \frac{P_A}{\sqrt{2\pi m_A k_b T}} \quad (3)$$

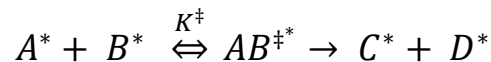
Where r_A is the rate of adsorption per unit area.

$\sigma(T)$ is the sticking coefficient or the probability that the collision of a molecule with the clean surface leads to adsorption and has a value between 0 and 1.

$f(\theta_r)$ is a function of surface coverage and takes into account the available surface sites for adsorption. θ_r is the reduced coverage and is the ratio of the surface coverage over the surface coverage at surface saturation.

P_A is the pressure of the gas. m_A represents the mass of gaseous species A and $T(K)$ is the temperature.

Transition state theory: Transition state theory assumes that an activated complex is formed from reactants before forming the products. The activation complex is the molecular structure that lies at the saddle point in the potential energy landscape between the reactants and products. This activated complex is generally referred to as the transition state. The critical assumption of transition state theory is that the transition state and the reactants of the elementary steps are in quasi-equilibrium, as shown below:



In this formulation, the reactants A* and B* form a transition state $AB^{\ddagger*}$, which is in equilibrium with the reactants. Using the equilibrium relation, the rate of forward reaction is obtained as:

$$\vec{r} = \vec{k} a_A a_B = \frac{k_B^* T}{h} * \exp\left(\frac{\Delta S^{0\ddagger}}{R}\right) * \exp\left(-\frac{\Delta H^{0\ddagger}}{RT}\right) * a_A a_B \quad (4)$$

Where k_B is the Boltzmann constant, h is the Plank's constant, a_A and a_B are the activities of the reactants A and B, respectively. $\Delta H^{0\ddagger}$ and $\Delta S^{0\ddagger}$ are the standard enthalpy change and standard entropy change for the formation of transition state from the reactants, respectively. $\Delta H^{0\ddagger}$ is generally referred as the activation barrier/energy of the elementary reaction.

From eq 2 backward rate constant can be estimated if the value of K_{eq} is known. Therefore to find out the forward and backward rate constants of an elementary reaction using TST, we require $\Delta H^{0\ddagger}$, $\Delta S^{0\ddagger}$, ΔH^0 and ΔS^0 which can be obtained from Density functional theory (DFT) methods. In addition, the Unity bond index-quadratic exponential potential (UBI-QEP) method is an analytical method for determining ΔH^0 and $\Delta H^{0\ddagger}$.

2.1.4 Microkinetic model development

The rate of change of the surface coverage (θ_j) of a reaction intermediate is determined by the rate of production and consumption of the intermediate:

$$\frac{\partial \theta_j}{\partial t} = \sum_i v_{ij} r_i \quad (5)$$

An additional constraint is the conservation of surface sites; that is, the sum of all surface coverages must equal 1:

$$1 = \theta_* + \sum_j n_j \theta_j \quad (6)$$

Where v_{ij} , is the stoichiometric coefficient of species j in the elementary step i . r_i is the rate expression for reaction step i . θ_* is the concentration of free sites, and n_j is the number of surface sites occupied by the j^{th} intermediate.

Equations 5 and 6 can be solved together for a known gaseous species pressure to see the surface coverages variation with time and its value at a steady state. Also, these equations can be coupled with material balance for the gas species (within a reactor system) to obtain the outlet gas species concentration, which is shown in section 4.4.2 of this work.

3. Literature survey

The most commonly used mechanism to describe catalytic dehydrogenation is the reverse Horiuti–Polanyi mechanism proposed in 1934.^[21] In this mechanism, the dehydrogenation of alkanes is considered to consist of three steps: (i) dissociative alkane adsorption in which one hydrogen atom is removed, (ii) β -hydrogen abstraction of the adsorbed hydrocarbon species and formation of the double bond, and (iii) desorption of the alkene species and H_2 .^[21] Horiuti and Polanyi also described the possibility of side reactions of the adsorbed alkene species on the surface by deep dehydrogenation reactions. However, a detailed understanding of the reaction mechanism is still elusive. We have conducted an extensive literature survey for propane dehydrogenation (PDH) on the surface of Pt-based catalysts to understand the PDH reaction pathway.

Pt and Pt-based alloys have long been known as important catalysts in the hydrogenation of olefins and the dehydrogenation and paraffin' cracking.^[4,7] However, the major problem for Pt-based catalysts is the C–C cleavage of long-chain hydrocarbons, leading to coke formation. As a result, the catalyst loses its activity quickly and must be regenerated, which increases the process complexity. In the propane dehydrogenation system, it is vital to understand the reaction mechanism to improve propylene selectivity and suppress coke formation. Yang et al.^[4,8] has conducted DFT study and presented the elementary reaction network of propane dehydrogenation over closed packed Pt(111), stepped Pt(211), and Pt-Sn surfaces. Zan Lian et al.^[9] have revealed the Janus character of the coke precursor in the PDH on Pt catalysts from a KMC simulation and conducted DFT. Su and coworkers^[9] also gave a complete description of dehydrogenation's reaction pathway to propylene, deep dehydrogenation, and C–C bond cracking on a Pt (111) surface. Stephanie Saerens^[16] group has also investigated the PDH on Pt catalyst and presented an extensive reaction scheme to describe the effect of hydrogen on the increasing propylene selectivity. In the next section, surface reactions and DFT results from the literature are analyzed to better understand the reaction pathway for PDH on the Pt catalyst.

3.1 Adsorption of propane and propylene

The interactions between the reactant (propane) and product (propylene) with catalysts have apparent importance for PDH. Zan Lian et al.^[9] has employed BEEF-vdW exchange-correlation functional to calculate the binding energy of propane on Pt(111) and found that propane is weakly physisorbed on the surface of Pt with adsorption energy of -0.30 eV. Yang et al.^[4,8] has also stated that molecular propane is repelled by the metal surface, drifting over the Pt surface, and propane cannot bind to the Pt atoms, and the adsorption energy is -0.04 eV. The above results show that propane is weakly physisorbed on Pt(111) and Pt(211).

The LEED analysis^[46] indicated that propylene could be adsorbed at the Pt surface in both the di- σ and π -mode (Figure 2). Valcárcel et al.^[11] performed DFT calculation on Pt(111) and reported that propylene gets chemisorb at the bridge site in di- σ mode. In Yang et al.^[4,8] calculations, the adsorption energy in the di- σ mode on Pt(111) is 0.27 eV higher than that in the π -mode, which is consistent with the results of Zaera and Chrysostomou.^[47] Propylene is preferentially adsorbed at the Bridge site by binding with two Pt atoms. On the stepped surface, propylene also favors the Bridge site on the step edge, and the optimized structure is similar to that on the flat surface. However, the adsorption energy is calculated to be -1.17 eV, 0.83 eV higher than that on the flat surface, indicating that binding to the less coordinated Pt atoms is preferred.

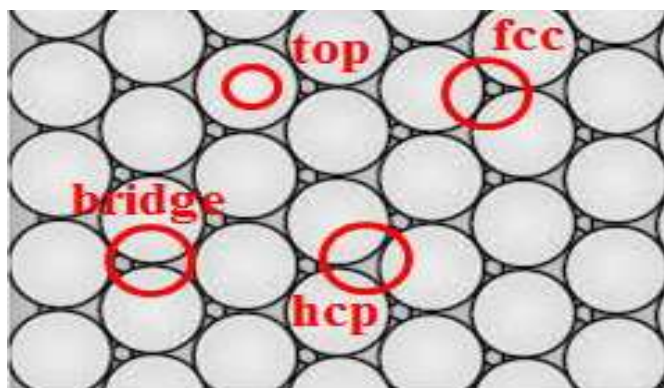


Figure 2: Adsorption sites on Pt(111) catalyst^[19]

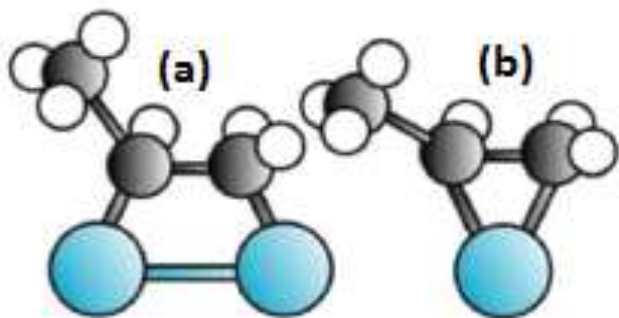


Figure 3: Adsorption modes of propylene on Pt(111): (a) di- σ mode, (b) π mode Light blue: Pt atoms, Black: C atoms, White: H atoms^[5]

3.2 Propane dehydrogenation to form propylene

On the catalyst surface, propane gets converted into propylene and hydrogen via a two-step process^[13, 14]:

- 1) C-H bond activation at methyl and methylene group to produce 1-propyl and 2-propyl, respectively.
- 2) β – Dehydrogenation of 1-propyl and 2-propyl to form propylene.

Each detached hydrogen atom requires an empty site for accommodation. Therefore, it is reasonable to expect that the hydrogen coverage would significantly affect the dehydrogenation activation energy^[4,8].

In step 1, the energy barriers for the initial activation of propane at both the methyl and methylene groups are calculated to be 0.69 and 0.70 eV^[4,8] on Pt(111), respectively. The activation energy is only 0.01 eV higher than that for the dehydrogenation of the methyl group, indicating no preference for the activation of C–H bonds. In step 2, the activation energies for the dehydrogenation of 1-propyl and 2-propyl are calculated to be 0.70 and 0.68 eV^[4,8], respectively, which indicates that the dehydrogenation of both 1-propyl and 2-propyl is kinetically favorable to produce propylene.

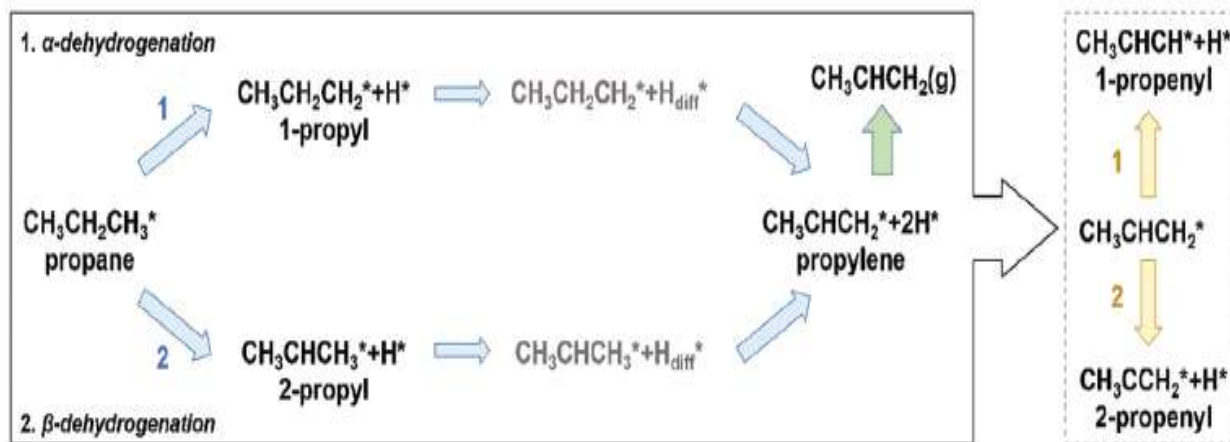


Figure 4: Simplified network for propane dehydrogenation to form propylene^[14].

In the case of step sites, the energy barriers for the initial activation of propane occurring at the methyl and methylene groups are calculated to be 0.32 and 0.28 eV^[4,8], respectively. The subsequent dehydrogenation takes place at the edge bridge site, and the energy barriers for the activation of 1-propyl and 2-propyl are 0.34 and 0.33 eV^[4,8], respectively. Comparison between activation energy at Pt(111) and Pt(211) leads to finding that Pt(211) is more active for propane dehydrogenation.

3.3 Deep dehydrogenation

3.3.1 Dehydrogenation of propylene and formation of Propylidyne

Chen et al. and Honkala et al.^[13] showed that the competition between C_3H_6 desorption and C_3H_6 dehydrogenation can be used for propylene selectivity. On Pt(111), di- σ adsorb propylene gets

dehydrogenated at methylene group with detached H atom at atop site and product 1-propenyl on fcc site (energy barrier of 0.76 eV).^[15] A similar energy barrier (0.77 eV) was observed for the formation of 2-propenyl. Propylene gets quickly dehydrogenated at stepped Pt (0.29-0.40 eV), which shows lower propylene selectivity of Pt(211) as compared to Pt(111).

1-propylidene can easily dehydrogenate to form Propylidyne (0.23 eV, lower than other dehydrogenation)^[15]. Further dehydrogenation or hydrogenation of Propylidyne requires high energy, suggesting that Propylidyne is the most favorable intermediate on Pt(111). However, on Pt(211) energy barrier is 0.52 eV higher than Pt(111).

3.3.2 C-C cracking of C₃ intermediates

C-C cleavage forms less stable products relative to dehydrogenated products. As shown in the reaction scheme proposed by Stephanie Saerens^[19] group, almost all the C-C scission have an activation barrier of greater than 140 KJmol⁻¹, and thus these C-C scission reaction steps are not favorable. The most important exception is the C–C scission of propyne, which is responsible for the formation of the side products through deep dehydrogenation and further C–C scission reactions^[4,8]. Propyne cracking is the starting point to form methylidyne and ethylidyne, which ultimately produce the species like methane, ethane, ethylene, and coke, thus affecting the propylene selectivity and deactivation of the catalyst.

4. Statement of the problem

Understanding the complex nature of propane dehydrogenation on Pt catalyst and proposing a reaction scheme consists of elementary reactions based on a combination of literature and chemical intuition. Kinetic simulation in a PFR reactor model is performed using the proposed reaction scheme. The results of the simulations are compared with the experimental outcomes by Siddiqi et al.^[19]

4.1 Reaction Scheme proposed for PDH on Pt catalyst in this work

As discussed in the introduction section, Pt-based catalyst is used in the propane dehydrogenation (PDH) process. However, the main problem occurs with Pt catalyst: it needs to be regenerated periodically. In PDH, apart from the primary reaction of catalytic conversion of propane into propylene and hydrogen, there are side reactions which also occurs at high temperature operating condition and thus result in the formation of side products which ultimately occupy the active sites of the catalyst and deactivate the surface of the catalyst. These side products also lower the selectivity of propylene. The complex nature of PDH and side reactions (deactivation and Cracking reactions) requires fundamental insight into the reaction mechanism.

Horiuti-Polanyi^[21] has proposed the reaction mechanism to describe catalytic dehydrogenation in 1934, which is commonly used. For alkane dehydrogenation, they have considered three steps: (a) dissociative alkane adsorption in which one hydrogen atom is removed, (b) β -hydrogen abstraction of the adsorbed hydrocarbon species, and formation of the double bond, and (c) desorption of the alkene species and H_2 ^[21]. Horiuti and Polanyi also described the possibility of side reactions of the adsorbed alkene species on the surface by deep dehydrogenation reactions.

Yang et al.^[4, 8] conducted a DFT study and presented the elementary reaction steps of 29 surface reaction steps for propane dehydrogenation over the Pt catalyst. At the same time, Yang et al. has considered the C-C scission but only for C_3 species, not for C_2 species. Stephanie Saerens^[19, 20] group has also investigated the PDH on Pt catalyst and presented an extensive reaction scheme of 42 surface reaction steps and 6 adsorption/desorption reaction that includes isomerization reactions and C-C scission of both C_3 and C_2 intermediates. Zan Lian et al.^[19] have revealed the Janus character of the coke precursor in the PDH on Pt catalysts from a KMC simulation and conducted DFT for the same. They have proposed a set of 45 elementary reactions to describe PDH. A detailed understanding of the reaction mechanism is still elusive for PDH. The rate-determining step (RDS) for the PDH is still unclear as some authors have considered the dissociative adsorption as RDS. In contrast, others suggest the β - hydrogen abstraction as the rate-determining step^[22, 23, 24]. Additionally, the exact mechanism of coke formation is not clearly mentioned since the actual coke formation mechanism is very complex and too elaborate to include in an ab initio network, as also discussed in the work of Zhao et al.^[25]. Li et al.^[23] have included both C-C scission and oligomerization reactions in their kinetic model on a Pt-Sn catalyst. Others claim that the rate-

determining step for the coke formation is coke precursor formation through propylene oligomerization.^[26, 27]

In this work, we have proposed a reaction network, as shown in Table 2 and Figure 5, which consists of 23 surface reactions and 6 adsorption/desorption reactions based on a combined literature survey and chemical intuition. In our proposed reaction network, we have considered mainly the following type of reactions:

- (i) Adsorption and desorption of gas-phase species (Ra, Rb, Rc, etc.)
- (ii) Dehydrogenation reactions in which a hydrogen atom is removed from a hydrocarbon species on the surface (R1 – R6)
- (iii) C–C scission reactions in which two hydrocarbon species are formed on the surface (R13, R14)
- (iv) Deep dehydrogenation reactions in which a hydrogen atom is abstracted from a hydrocarbon species which is propylene or beyond propylene (R7-R12, R15-R17)

We have 6 gas species and 20 surface intermediates shown in Table 3(a) and Table 3(b).

We have not considered the polymerization reactions proposed in the literature as the activation energy for those are higher than 140 KJ/mol^[16], which are relatively large compared to other reactions as given in our reaction scheme. A DFT study on ethane dehydrogenation performed by Chen et al. confirms the energetically unfavorable isomerization reactions.^[28] C–C scission of propyne (CHCCH3) is included as it produces methylidyne (CH) and ethylidyne (CCH3), which is the starting point for the formation of side products such as methane, ethane, and ethylene. C–C scission reactions only occur with more dehydrogenated species than propylene, as already suggested by Yang et al.^[4,8]

Thermodynamic and kinetic data required for the elementary reactions are adapted from the paper of Stephanie Saerens et al.^[19] at the temperature of 873 K. Enthalpies and entropies for all intermediates and transition states are estimated by this group based on DFT calculations. The adsorption enthalpies and entropies of the products propylene, methane, ethane, ethylene, and hydrogen have been adapted so that the overall calculated gas-phase reaction equilibrium is consistent with that derived from NIST reference values. Furthermore, Arrhenius activation energies (E_a) and pre-exponential factors (A) for the reaction steps were calculated from transition-state theory (TST). Thermodynamic consistency is maintained by calculating the backward rate constant using the equilibrium rate constant throughout the process. For alkanes (C3H8, C2H6, and CH4), physisorption is assumed to be equilibrated, and the physisorption is lumped with the consecutive dissociative adsorption steps^[12, 13].

Table 2: Thermodynamic and kinetic data at T = 873 K for all the reactions steps proposed in the reaction scheme for PDH on Pt catalyst

Elementary reaction steps	ΔH_r^0	ΔS_r^0	$E_{a(f)}$	A_f	k_f	K_{eq}
(1) C_3H_8 (physisorbed) + * \rightleftharpoons $CH_2CH_2CH_3$ (1-propyl) + H^*	-14	-45	72	1.3×10^{10}	9.2×10^6	3.1×10^{-2}
(2) C_3H_8 (physisorbed) + * \rightleftharpoons CH_3CHCH_3 (2-propyl) + H^*	-22	-55	58	2.0×10^{10}	8.4×10^6	2.6×10^{-2}
(3) $CH_2CH_2CH_3$ (1-propyl) + * \rightleftharpoons $CHCH_2CH_3$ (1-propylidene) + H^*	-1	-12	74	2.6×10^{12}	1.3×10^8	2.8×10^{-1}
(4) $CH_2CH_2CH_3$ (1-propyl) + * \rightleftharpoons CH_2CHCH_3 (propylene) + H^*	-30	-29	71	9.6×10^{12}	7.5×10^8	1.7×10^0
(5) CH_3CHCH_3 (2-propyl) + * \rightleftharpoons CH_3CCH_3 (2-propylidene) + H^*	7	-1	84	4.7×10^{12}	6.0×10^7	3.5×10^{-1}
(6) CH_3CHCH_3 (2-propyl) + * \rightleftharpoons CH_2CHCH_3 (propylene) + H^*	-22	-19	75	1.7×10^{13}	7.0×10^8	2.1×10^0
(7) CH_2CHCH_3 (propylene) + * \rightleftharpoons $CHCHCH_3$ (1-propenyl) + H^*	11	9	82	1.2×10^{13}	2.2×10^8	6.5×10^{-1}
(8) CH_2CHCH_3 (propylene) + * \rightleftharpoons CH_2CCH_3 (2-propenyl) + H^*	-2	14	73	1.3×10^{13}	7.6×10^8	6.2×10^0
(9) $CHCH_2CH_3$ (1-propylidene) + * \rightleftharpoons $CHCHCH_3$ (1-propenyl) + H^*	-18	-8	64	3.3×10^{12}	6.4×10^8	4.1×10^0
(10) CH_3CCH_3 (2-propylidene) + * \rightleftharpoons CH_2CCH_3 (2-propenyl) + H^*	-31	-5	59	3.9×10^{12}	1.4×10^9	3.7×10^1
(11) $CHCHCH_3$ (1-propenyl) + * \rightleftharpoons $CHCCH_3$ (propyne) + H^*	-19	9	80	5.4×10^{13}	1.2×10^9	3.6×10^1
(12) CH_2CCH_3 (2-propenyl) + * \rightleftharpoons $CHCCH_3$ (propyne) + H^*	-6	4	78	7.5×10^{12}	2.2×10^8	3.8×10^0

Elementary reaction steps	ΔH_r^0	ΔS_r^0	$E_{a(f)}$	A_f	k_f	K_{eq}
(13) CHCCH_3 (propyne) + * \rightleftharpoons CCH_3 (ethynylidyne) + CH (methynylidyne)	-67	-1	111	2.7×10^{13}	1.0×10^7	6.7×10^3
(14) CCH_3 (ethynylidyne) + * \rightleftharpoons C (atomic carbon) + CH_3 (methyl)	81	-8	185	2.9×10^{13}	5.1×10^2	7.6×10^{-6}
(15) CH_3 (methyl) + * \rightleftharpoons CH_2 (methynylidene) + H^*	20	4	86	1.2×10^{13}	1.2×10^8	1.1×10^{-1}
(16) CH_2 (methynylidene) + * \rightleftharpoons CH (methynylidyne) + H^*	-54	0	24	4.7×10^{12}	1.9×10^{11}	1.4×10^3
(17) CH (methynylidyne) + * \rightleftharpoons C (atomic carbon) + H^*	50	8	123	1.9×10^{13}	1.4×10^6	3.2×10^{-3}
(18) CH_2CH_3 (ethyl) + * \rightleftharpoons CHCH_3 (ethynylidene) + H^*	12	21	88	1.2×10^{14}	9.4×10^8	2.6×10^0
(19) CHCH_3 (ethynylidene) + * \rightleftharpoons CCH_3 (ethynylidyne) + H^*	-73	4	22	2.7×10^{12}	1.6×10^{11}	2.6×10^4
(20) * C (atomic carbon) \rightarrow graphitic coke formation + *					3.1×10^3	
(21) CH_3 (methyl) + H^* \rightleftharpoons CH_4 (physisorbed)	18	105	91	2.9×10^{14}	1.5×10^9	2.8×10^4
(22) CH_2CH_3 (ethyl) + H^* \rightleftharpoons CH_3CH_3 (physisorbed)	28	91	90	5.4×10^{14}	3.1×10^9	1.3×10^3
(23) CH_2CH_3 (ethyl) \rightleftharpoons CH_2CH_2 (ethylene) + H^*	-14	15	92	1.0×10^{15}	4.8×10^9	3.8×10^1
(a) C_3H_8 (g) + * \rightleftharpoons C_3H_8 (physisorbed)	-34	-84			1.3×10^8	3.9×10^{-3}
(b) C_3H_6 (g) + * \rightleftharpoons C_3H_6 (chemisorbed)	-109	-185			1.4×10^8	4.6×10^{-4}
(c) H_2 (g) + 2* \rightleftharpoons 2 H^*	-101	-114			2.0×10^8	8.1×10^{-1}
(d) CH_4 (g) + * \rightleftharpoons CH_4 (physisorbed)	-18	-20			2.2×10^8	1.0×10^0

Elementary reaction steps	ΔH_r^0	ΔS_r^0	$E_{a(f)}$	A_f	k_f	K_{eq}
(e) $C_2H_6(g) + * \rightleftharpoons C_2H_6(\text{physisorbed})$	-27	-60			1.6×10^8	2.7×10^{-2}
(f) $C_2H_4(g) + * \rightleftharpoons C_2H_4(\text{chemisorbed})$	-111	-156			1.7×10^8	2.0×10^{-2}

Units: ΔH_r^0 and $E_{a(f)}$ are in **KJmol⁻¹** ΔS_r^0 in **Jmol⁻¹ K⁻¹** A_f and k_f are in **s⁻¹** or **bar⁻¹s⁻¹**

* The essence of reaction no. 20 is to prevent accumulation of the thermodynamically very stable atomic carbon, and it is assumed that all formed graphitic coke migrates immediately to the support. The rate constant of this irreversible reaction is taken from the work of Stephanie Saerens et al. ^[19]

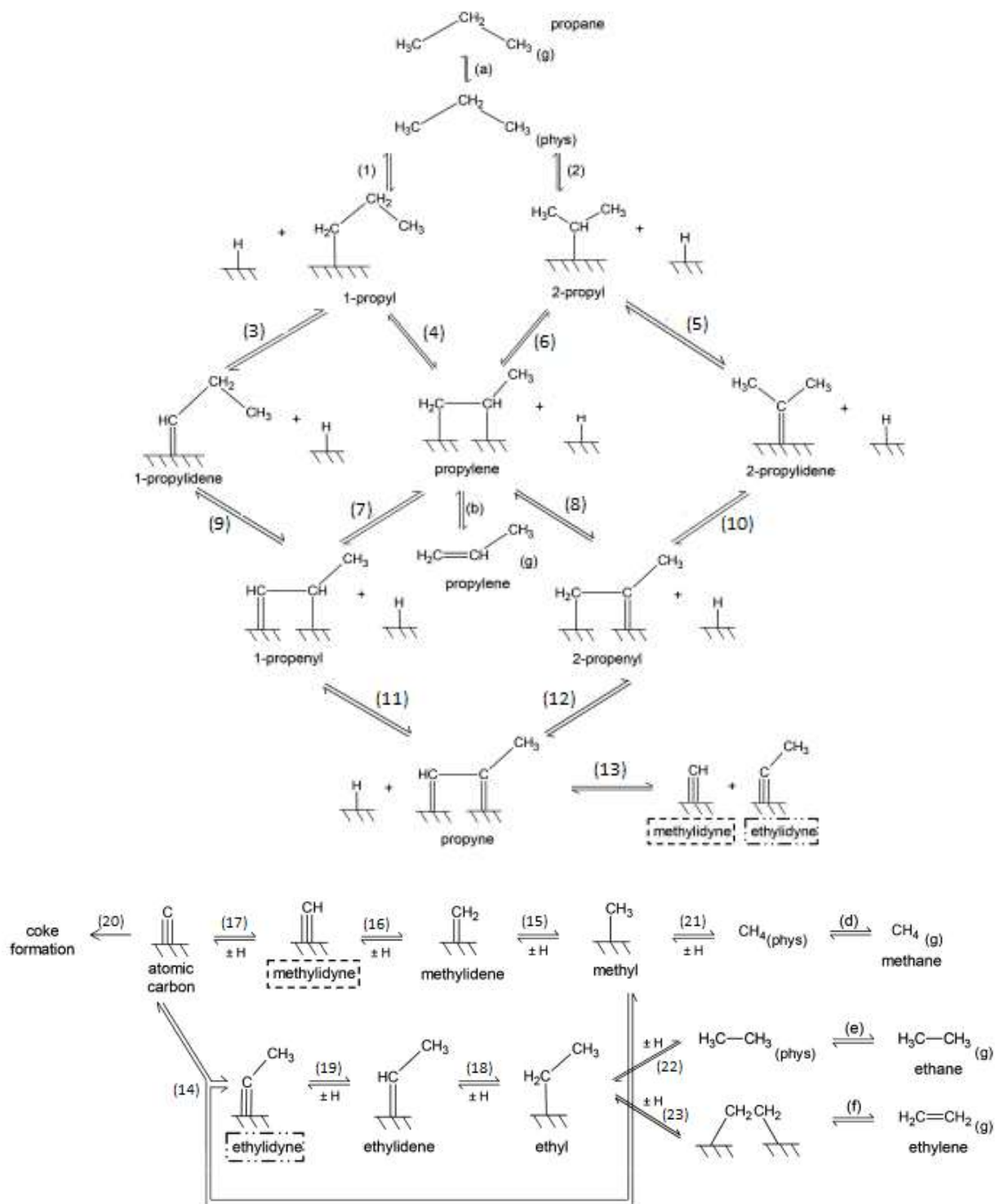


Figure 5: Reaction scheme for propane dehydrogenation as described in Table 2. “phys” stands for the physisorbed species. The species that provide the link between the top and the bottom schemes are shown in boxes.

Table 3(a): Gas species present in the reaction network with their chemical

S.R.No	Gas Species	Chemical Notation
1	Propane	C_3H_8 (g)
2	Propylene	C_3H_6 (g)
3	Methane	CH_4 (g)
4	Hydrogen	H_2 (g)
5	Ethane	C_2H_6 (g)
6	Ethylene	C_2H_4 (g)

Table 3(b): Surface intermediates present in the reaction network with their chemical notations

S.R.No	Surface Intermediates	Chemical Notation
1	Hydrogen	H^*
2	1-Propyl	$CH_2CH_2CH_3$
3	2-Propyl	CH_3CHCH_3
4	1-Propylidene	$CHCH_2CH_3$
5	2-Propylidene	CH_3CCH_3
6	Propylene (Chemisorbed)	CH_2CHCH_3
7	1-Propenyl	$CHCHCH_3$
8	2-Propenyl	CH_2CCH_3
9	Propyne	$CHCCH_3$
10	Ethylidyne	CCH_3
11	Methylidyne	CH
12	Atomic carbon	C
13	Methyl	CH_3
14	Methylidene	CH_2
15	Ethyl	CH_2CH_3
16	Ethylidene	$CHCH_3$
17	Ethylene (Chemisorbed)	CH_2CH_2
18	Propane (Physisorbed)	C_3H_8 (physisorbed)
19	Ethane (Physisorbed)	C_2H_6 (physisorbed)
20	Methane (Physisorbed)	CH_4 (physisorbed)
21	Surface vacancy	*

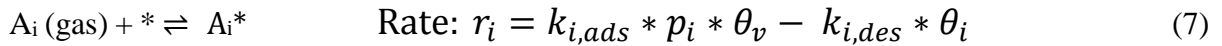
4.2 Modeling of reactions

4.2.1 Formulation of rate laws

The reactions considered in our work are of mainly two types based on differences in writing the mathematical expressions for the rate laws: (1) adsorption and desorption of gas-phase species (2) surface reactions, i.e. dehydrogenation or C-C scission reactions.

Rate laws are formulated in mathematical expressions for a different types of reactions as follows:

(1) Adsorption and desorption of gas-phase species i :



Where, $k_{i,ads}/k_{i,des}$ are the rate coefficient of adsorption and desorption. ($\text{bar}^{-1}\text{s}^{-1}$ or bar^{-1}).

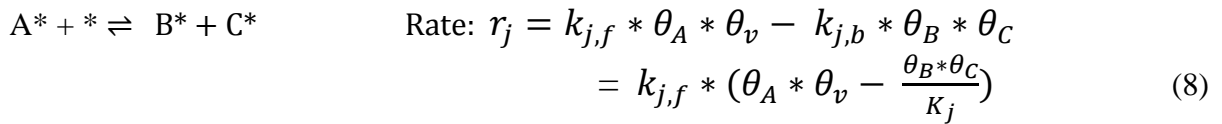
p_i is the partial pressure of gas species i (bar).

The fractional coverage θ_i of species i is defined as the number of adsorbate molecules i per number of Pt surface atoms (moles of adsorbate i per moles of Pt surface atoms).

θ_v is the fractional coverage of vacant/free sites.

In H_2 adsorption, eq 7 has twice θ^2 instead of θ since H_2 adsorbs dissociatively on the surface.

(2) Surface reactions (Dehydrogenation or C-C scission reactions):



Where $K_j = \frac{k_{j,f}}{k_{j,b}}$

K_j is the equilibrium constant of the j th surface reaction.

NOTE: For alkanes (C_3H_8 , C_2H_6 , CH_4), physisorption is assumed to be equilibrated, and the physisorption is lumped with the consecutive dissociative adsorption steps.

Example: for the dissociative adsorption of C_3H_8 to form 1-propyl and hydrogen, this leads to the following expressions:





$$r_1 = k_{1,f} * (\theta_{\text{C}_3\text{H}_8(\text{phy})} * \theta_v - \frac{\theta_{1\text{-propyl}} * \theta_{\text{H}^*}}{K_1}) \quad (10)$$

Replacing the value of $\theta_{\text{C}_3\text{H}_8(\text{phy})}$ in eq 10 from eq 9, we get

$$r_1 = k_{1,f} * (K_a * p_{\text{C}_3\text{H}_8} * \theta_v^2 - \frac{\theta_{1\text{-propyl}} * \theta_{\text{H}^*}}{K_1}) \quad (11)$$

4.2.2 Microkinetic and reactor model

In section 2.2.4 microkinetic model for the surface intermediates are given, and variation of surface coverage with respect to time at constant gas pressure can be found by solving coupled ODE's (eq 5) and conservation of surface site (eq 6). However, to account for the change in the gas phase composition, we need to couple the microkinetic model with the reactor model.

Reactor model: We have chosen an ideal plug flow reactor (PFR) to model the reactor since it is used in the experimental studies by Siddiqi et al.^[19] The plug flow reactor model is solved for the flow rates of the gas-phase species i :

$$\frac{dF_i}{dW} = R_i = \sum_j v_{ji} r_j \quad \text{Initial condition: } F_i(0) = F_{i0} \quad (12)$$

F_i being the molar flow of gas-phase species i in mol/sec.

W the catalyst mass in grams.

R_i the net rate of production of species i per catalyst unit mass.

F_{i0} is the initial molar flow rate of species i in mol/sec.

v_{ij} , is the stoichiometric coefficient of species i in the elementary step j

Microkinetic model: Pseudo steady-state approximation (*PSSA*) is applied for every surface intermediates thus resulting in a set of algebraic equations:

$$\frac{d\theta_j}{dt} = 0 = R_j = \sum_i v_{ij} r_i \quad (13)$$

Furthermore, the sum of all fractional surface coverages amounts to 1

$$\theta_v + \sum_i \theta_i = 1 \quad (14)$$

Altogether eq 12, 13, and 14 describe the whole model and forms the differential-algebraic equations (DAE) system, which is solved in the Athena Visual Studio with its inbuilt DAE solver.

NOTES:

(1) We have assumed the ideal gas behavior of gaseous species. So we can write

$$p_i = C_i * R * T \quad (15)$$

$$F_i = C_i * v \quad (16)$$

Combining eq 15 and eq 16 leads to a relationship between molar flow rate and partial pressure of species i in the following manner

$$p_i = \frac{F_i * R * T}{v} \quad (17)$$

Where v is the volumetric flow rate of the inlet stream in $\text{m}^3\text{sec}^{-1}$

R is the gas constant and equal to $8.314 * 10^{-5} \text{ m}^3\text{bar/mol K}$

T is the temperature in kelvins (K)

(2) To maintain the correct dimension of RHS and LHS in eq 6, all the rates (r_i) as described in section 4.2.1 are multiplied by a factor which is equal to $3 * 10^{-5} (n_{\text{Pt}})$, and it has a dimension of moles of Pt surface sites per gram of catalyst. This factor is calculated from the work of Siddiqi et al.^[19] and shown in the further section.

(3) Definition of terms that are used in this work to compare the simulation results with the experimental outcomes

$$\text{Conversion (X) of the propane: } X = \frac{F_{C_3H_8,in} - F_{C_3H_8,out}}{F_{C_3H_8,in}} \quad (18)$$

$$\text{Selectivity (S}_{C_xH_y}\text{): } S_{C_xH_y} = \frac{F_{C_xH_y,out}}{F_{C_3H_8,in} - F_{C_3H_8,out}} * \frac{x}{3} \quad (19)$$

Site time yields (STYs): Number of molecules of a specified product produced per Pt surface atom and per unit time over the whole reactor.^[29]

$$STY_S = \frac{F_{C_3H_6}}{n_{Pt}} \quad (20)$$

Where $F_{C_3H_8,in}$ is the inlet molar flow rate of propane in moles/sec.

$F_{C_3H_8,out}$ is the molar flow rate of propane at the outlet in moles/sec.

n_{Pt} represent the number of Pt surface sites. STYs is in units of $\text{mol}_{C_3H_6} \text{mol}_{Pt \text{ sites}}^{-1} \text{s}^{-1}$

4.3 Data collection from the work of Siddiqi et al.^[19,20]

The reaction conditions for the reactor simulations in this work are taken from the work of Siddiqi et al.^[19,20], who performed experiments on propane dehydrogenation on a Pt/Mg(Al)O catalyst in a plug flow reactor (Isothermal condition). In these experiments, a catalyst mass of 0.025 g was used at a reaction temperature of 873 K with 20 vol % propane in the feed at a total pressure of 1.013 bar. Balance He (inert) was added to obtain a total feed inlet flow rate of 10^{-6} m³/sec.

The microkinetic simulations performed in this work require input data that are not directly reported in the experimental literature of Siddiqi *et al.*^[19] such as initial molar flow rates of inlet species, the number of Pt surface sites (n_{Pt}). Furthermore, the site time yield (STY) and the conversion are also not reported explicitly, and these need to be compared to the output of the simulations.

For this simulation, we took the inlet ratio H₂/C₃H₈ of 1.25 as a reference since this ratio leads to the highest experimentally observed activity. To compare simulation results with experiment outcomes, time of stream (TOS) of 5 min is taken, which is assumed to be sufficiently large at which highly active but unselective under coordinated (step) sites are deactivated due to coke formation^[30,31]. A summary of input data required for simulation is given in Table 4.

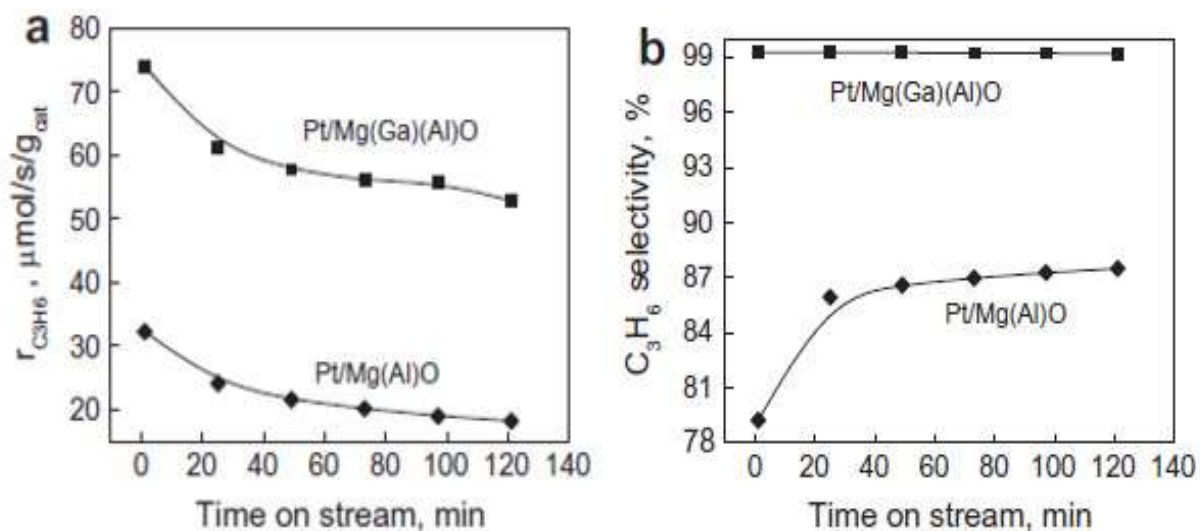


Figure 6: (a) Variation of the rate of propylene in $\mu\text{mol/s/g}_{\text{cat}}$ with respect to time on stream (min) (TOS) (b) Selectivity for propane dehydrogenation. Reaction temperature of 873 K, 20 vol% C₃H₈ in feed, H₂/ C₃H₈ = 1.25, with balance He for total flow rate of 10^{-6} m³/sec^[19].

4.3.1 Inlet molar flow rates of propane and hydrogen

The simulation requires the inlet molar flow rates of C₃H₈ and H₂ as input. A total feed flow rate of 10⁻⁶ m³/sec is reported consisting of 20 vol. % propane (at 1.013 bar and 298 K). Consequently, 0.2 m³/sec propane is fed to the reactor. Assuming all gas-phase species behave as ideal gasses, the feed flow rate of propane can be calculated as

$$F_i = \frac{P_i * v}{R * T} = \frac{0.2 * 1.013 * 10^5 * 10^{-6}}{8.314 * 298} = 8.177 * 10^{-6} \frac{mol}{s} \text{ (for propane)}$$

Similarly, a molar flow rate of 1.03×10^{-5} mol/s for hydrogen is calculated for H₂/C₃H₈ of 1.25

4.3.2 Calculation of n_{Pt}

Siddiqi *et al.* use the Pt/Mg(Al)O catalyst, but the number of Pt surface sites is not explicitly reported. Characterization of the same Pt/Mg(Al)O catalyst shows that a dispersion (D) of 84% is obtained^[20]. From the dispersion, the number of Pt surface sites (n_{Pt}) can be calculated using the below formula

$$n_{Pt} = \frac{wt.\% * m_{cat} * D}{MM_{Pt}}$$

Where m_{cat} is the weight of the catalyst, and $wt.\%$ is the weight percentage of Pt in the catalyst MM_{Pt} is the molar mass of Pt.

$$n_{Pt} = \frac{0.696 * 10^{-2} * 0.025 * 0.84}{195.078} = 7.492 * 10^{-7} \text{ mol of Pt surface sites}$$

➤ Or $3 * 10^{-5}$ mol of Pt surface sites per gram of catalyst.

4.3.3 Site time yield (STY)

The site time yield (STY) is not explicitly reported in the literature, but it can be calculated from the data given in the article^[19,20]. After 5 minutes of TOS, an activity of 30 μmol/s/g_{cat} on a Pt/Mg(Al)O catalyst is reported at a temperature of 873 K and H₂/ C₃H₈ feed ratio of 1.25. Based on the total catalyst mass (0.025 g) and the number of Pt surface atoms ($7.492 * 10^{-7}$) this leads to a STY of 1.0 mol_{C₃H₆}/s/mol_{Pt surf sites}.

4.3.4 Conversion

The inlet molar flow rate of propane is known and equal to 8.177×10^{-6} mol/sec, but outlet flow rates are unknown, so the reported yields are used to determine the conversion. After 5 minutes of TOS, the reported yield of C_3H_6 equals $30 \mu\text{mol/s/g}_{\text{cat}}$ as shown in Figure 6(a), on a Pt/Mg(Al)O catalyst, and the selectivity towards C_3H_6 at this point is reported to be ~80% as shown in Figure 6(b).

$$\text{From eq 18 } F_{C_3H_8,in} - F_{C_3H_8,out} = \frac{30 \times 10^{-6} \times 0.025}{0.8} = 9.375 \times 10^{-7} \text{ mol/sec}$$

And using eq 19, a conversion of 11.5% is calculated. Similar calculations are made for other conversion.

Table 4: Data required to perform simulation based on the experimental work by Siddiqi *et al.* [19,20]

Temperature	873 K
Total Pressure	1.013 bar
Catalyst weight	0.025 g
Molar inlet flow rate	
C_3H_8	8.177×10^{-6} mol/sec
H_2	1.03×10^{-5} mol/sec
Active sites	3×10^{-5} mol of Pt surface sites/g of catalyst

4.4 Solution of Differential algebraic equations (DAE) in Athena Visual Studio: Methodology

As discussed before, the reaction scheme proposed for PDH on Pt-based catalyst in this work results in the coupled ODE equations and algebraic equations, which were solved in the Athena Visual Studio in its inbuilt DAE solver.

All the species present in the reaction scheme are represented by variable $U(i)$ ($i=1-25$), which includes the molar flow rate of gas species and surface coverages (as defined in 4.2.1 section) of surface intermediates. The net rate of formation for each species is defined in the code. Also, all gas species' initial molar flow rates are given along with the initial guess of the surface coverages.

In its DAE solver number of equations are 25, and integration (w.r.t weight of the catalyst) starts from 0 and ends at either 4.53946×10^{-5} g (catalyst require for 11.5%) or higher weight ($>11.5\%$).

Athena code is attached in appendix A with appropriate comments, and the outcomes of this simulation are discussed in the next section

5. Results and discussion

The simulation has been performed using the coupled microkinetic and reactor model as discussed in section 4.2.2 and input data as summarized in Table X. Changing the weight of catalyst under constant inlet conditions results in conversion-selectivity profile as shown in Figure 8. For a fair comparison between simulation and experiment, the results are evaluated at the exact conversion, i.e., 11.5 % (obtained for TOS of 5 min), which required only 4.54×10^{-5} g of catalyst (in simulation). At the simulated conversion of 11.5%, the experiment and simulation results are compared and shown in Table 5.

Along with the main product, i.e., propylene, other side products such as methane, ethane, and ethylene have also been observed in the experiments by Siddiqi *et al.* ^[19]. At the conversion of 11.5% in the simulation, the selectivity of C_3H_6 , CH_4 , C_2H_6 , and C_2H_4 is 67.6%, 19.8%, 2.33%, and 10.1%, respectively, as shown in Figure 6.

Table 5: Comparison of simulation outcomes and experimental outcomes by Siddiqi *et al.* ^[19]

	Experiment	Simulation
Conversion %	11.5	11.5
Selectivity % (C_3H_6)	79.0	67.6
STY ($\text{mol}_{C_3H_6}/\text{s}/\text{mol}_{Pt \text{ surf sites}}$)	1.0	0.84

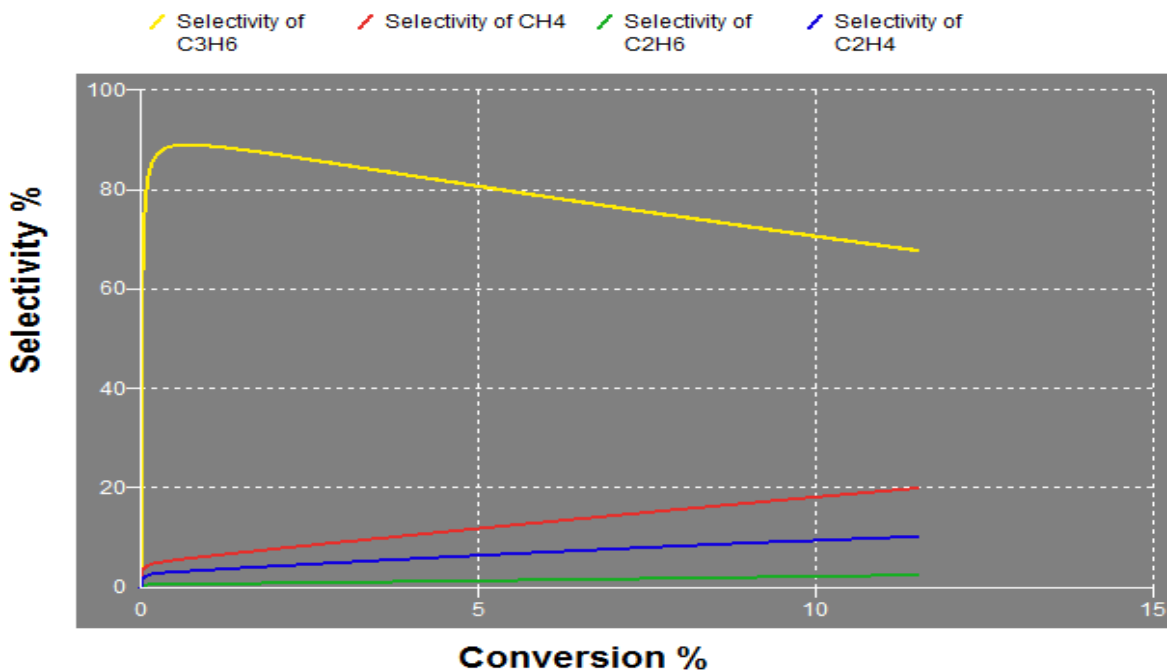


Figure 6: Selectivity of C_3H_6 , CH_4 , C_2H_6 , and C_2H_4 as a function of propane conversion from $X=0$ to $X=11.5\%$ (at $W = 4.54 \times 10^{-5}$ g, $H_2/C_3H_8 = 1.25$ and $T = 873K$).

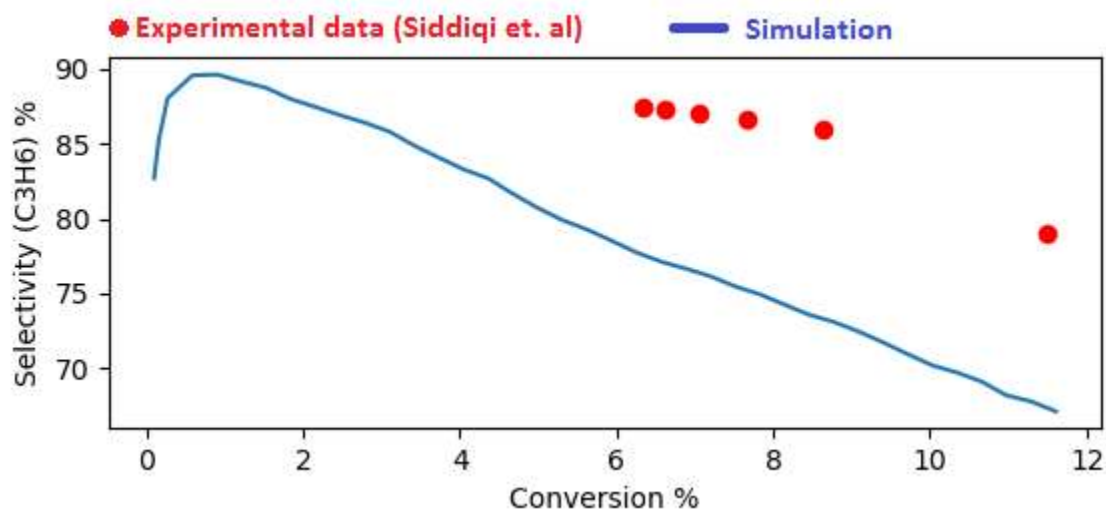


Figure 7: Comparison of experimental selectivity % of propylene with simulation selectivity

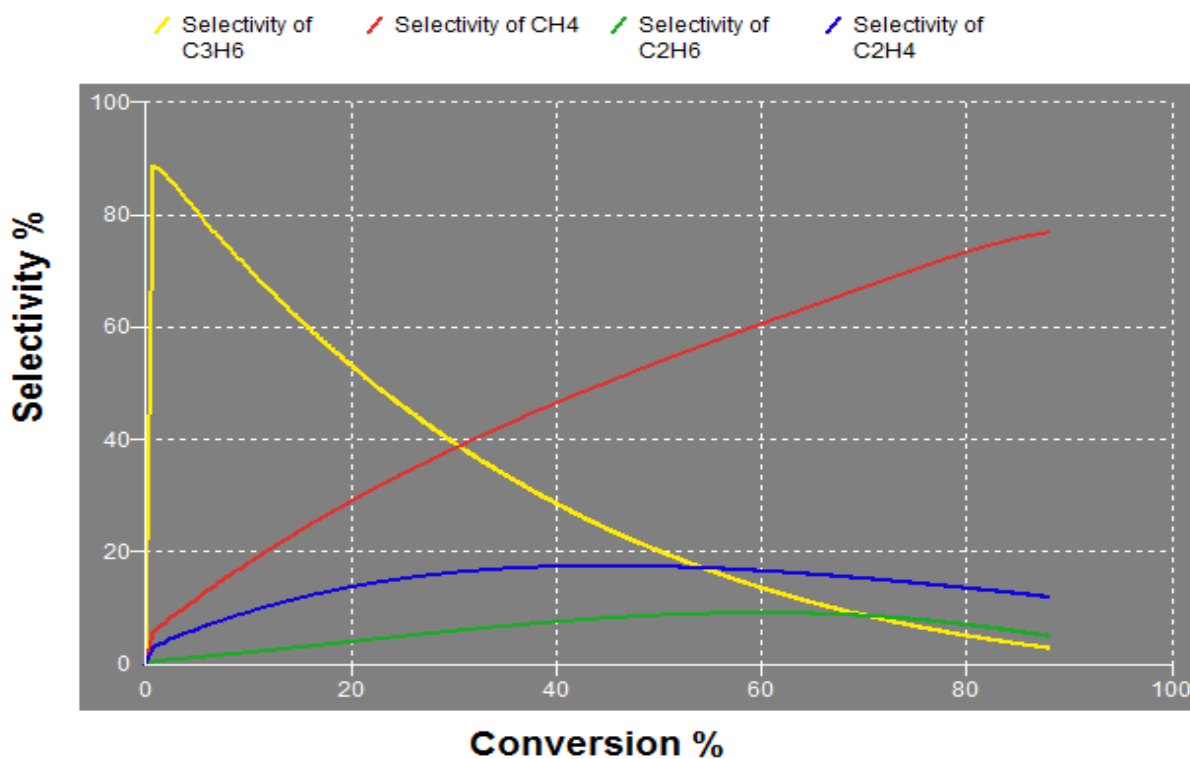


Figure 8: Selectivity of C₃H₆, CH₄, C₂H₆, and C₂H₄ as a function of propane conversion for higher conversion (at $W = 4.54 \times 10^{-5}$ g, $H_2/C_3H_8 = 1.25$ and $T = 873K$).

We have also compare the experimental selectivity of propylene with the simulated results at different conversion (Figure7) which reasonably explain the experiment outcomes of Siddiqi *et al.*^[19] qualitatively.

For conversion of 11.5%, the outlet molar flow rates of gaseous species (Table 6) were used to calculate the partial pressure of all gas species (Using eq 17). These partial pressure were further used to carry out the microkinetic simulation so that the surface coverages of all the surface intermediates can be observed as a function of time. Steady-state values of the surface coverages are reported in Table 6. Hydrogen (H*), ethylidyne (CCH₃), and methylidyne (CH) occupy most of the active sites on the catalyst surface at reactor outlet conditions. Ethylidyne and methylidyne are formed due to reaction 13, where propyne C-C scission occurs and is the starting point for the formation of side products (ethane, methane, and ethylene) and coke formation^[4, 8].

Table 6: Molar flow rates of gaseous species at conversion of 11.5% (at W = 4.54*10⁻⁵ g, H₂/C₃H₈ = 1.25 and T = 873K)

Species	C ₃ H ₈ (g)	C ₃ H ₆ (g)	CH ₄ (g)	H ₂ (g)	C ₂ H ₆ (g)	C ₂ H ₄ (g)
Molar flow rate (mol/sec)	7.13*10 ⁻⁶	6.28*10 ⁻⁷	5.51*10 ⁻⁷	1.06*10 ⁻⁵	3.25*10 ⁻⁸	1.40*10 ⁻⁶

Table 7: Surface coverages (steady state) at reactor outlet conditions for 11.5% conversion (at W = 4.54*10⁻⁵ g, H₂/C₃H₈ = 1.25 and T = 873K) with partial pressure of 0.52 bar C₃H₈, 0.045 bar C₃H₆, 0.77 bar H₂, 2.35*10⁻³ bar C₂H₆ and 0.01 bar C₂H₄.

S.R.No	Surface Intermediates	Surface coverages %
1	Hydrogen	28.18
2	1-Propyl	~ 0
3	2-Propyl	~ 0
4	1-Propylidene	~ 0
5	2-Propylidene	~ 0
6	Propylene (Chemisorbed)	~ 0
7	1-Propenyl	~ 0
8	2-Propenyl	0.005
9	Propyne	0.02
10	Ethylidyne	35.62
11	Methylidyne	0.53
12	Atomic carbon	~ 0

13	Methyl	~ 0
14	Methylidene	~ 0
15	Ethyl	~ 0
16	Ethylidene	0.001
17	Ethylene (Chemisorbed)	0.007
18	Propane (Physisorbed)	~ 0
19	Ethane (Physisorbed)	~ 0
20	Methane (Physisorbed)	~ 0
21	Surface vacancy	35.61

6. Future work

1) The proposed reaction scheme for PDH in this work reasonably satisfies the experiment outcomes of Siddiqi *et al.* ^[19]. However, to better understand the reaction pathway, sensitivity analysis can be applied to the microkinetic model to get information like the rate-determining step (RDS).

2) Our reaction scheme does not include the mechanism of coke formation, which is a drawback of our work and can be included in our reaction network to have a better insight into the exact mechanism of PDH.

References

- 1) Propylene from Propane via Dehydrogenation (similar to UOP Oleflex), <http://base.intratec.us/home/chemical-processes/propylene/propylene-from-propane-via-dehydrogenation>.
- 2) Propylene from Propane via Dehydrogenation (similar to Lummus CATOFIN), <http://base.intratec.us/home/chemicalprocesses/propylene/propylene-from-propane-via-dehydrogenation-2>.
- 3) US Department of Energy, Quadrennial Technology Review report, An Assessment of Energy Technologies and Research Opportunities, <https://energy.gov/sites/prod/files/2017/03/f34/qtr-2015-chapter6.pdf>, 2015.
- 4) M. L. Yang, Y. A. Zhu, C. Fan, Z. J. Sui, D. Chen, and X. G. Zhou.(2010). DFT study of propane dehydrogenation on Pt catalyst: effects of step sites. *Chem. Phys.*, 2011, 13, 3257–3267.
- 5) Sai Chen, Xin Chang, Guodong Sun, Tingting Zhang, Yiyi Xu, Yang Wang, Chunlei Pei, and Jinlong Gong (2021). Propane dehydrogenation: catalyst development, new chemistry, and emerging technologies. *Chem. Soc. Rev.*, 2021, Advance Article.
- 6) Ali Hussain Motagamwala and James A. Dumesic (2021). Microkinetic Modeling: A Tool for Rational Catalyst Design. *Chem. Rev.* 2021, 121, 2, 1049–1076.
- 7) C.L. Yu, Q.J. Ge, H.Y.Xu, W.Z. Li, Effects of Ce addition on the Pt-Sn/Al₂O₃ catalyst for propane dehydrogenation to propylene, *Applied Catalysis A: General* 315 (2006) 58-67.
- 8) M. L. Yang, Y. A. Zhu, C. Fan, Z. J. Sui, D. Chen, and X. G. Zhou.(2012). First-principles calculations of propane dehydrogenation over Pt-Sn Catalyst. *ACS Catal.* 2012, 2, 6, 1247–1258.
- 9) Z. Lian, S. Ali, T. Liu, C. Si, B. Li and D. S. Su. Revealing the Janus Character of the Coke Precursor in the Propane Direct Dehydrogenation on Pt catalyst from a kMC simulation *ACS Catal.*, 2018, 8, 4694–4704.
- 10) J. C. Wang, Effects of surface step on molecular propane adsorption, *Surface Science*, 2003, 540, 326.
- 11) Valcarcel A, Gil A, Ricart JM, Clotet A. Theoretical study of propene adsorbed on sulphated Pt(111). *Chemical physical Letters* 399 (2004) 295-299.
- 12) L. Nykanen and K. Honkala, Density Functional Theory Study on Propane and Propene Adsorption on Pt(111) and Pt-Sn Alloy Surfaces, *J. Phys. Chem. C*, 2011, 115, 9578–9586.

- 13)** L. Nykanen and K. Honkala, Selectivity in Propene Dehydrogenation on Pt and Pt₃Sn Surfaces from First Principles, *ACS Catal.*, 2013, 3, 3026-3030.
- 14)** R. J. Koestner, J. C. Frost, C. Stair, M. A. V. Hove, and G. Somorjai, *Surf. Sci.*, 1982, 116, 85.
- 15)** A. Valcarcel, J. Ricart, A. Clotet, A. Markovits, and C. Minot, *J. Catal.*, 2006, 241, 115.
- 16)** Stephanie Saerens, Maarten K. Sabbe, Vladimir V. Galvita, Evgeniy A. Redekop, Marie-Françoise Reyniers, and Guy B. Marin, The positive role of hydrogen on the propane dehydrogenation on Pt(111), *ACS Catal.* 2017, 7, 7495-7508
- 17)** Florian Karst, Matteo Maestri, Hannsjörg Freund, Kai Sundmacher, Reduction of microkinetic reaction models for reactor optimization exemplified for hydrogen production from methane, *Chemical Engineering Journal* 281 (2015) 981–994
- 18)** Thiago P. de Carvalho, Rafael C. Catapan, Amir A. M. Oliveira, and Dionisios G. Vlachos, Microkinetic Modeling and Reduced Rate Expression of the Water–Gas Shift Reaction on Nickel, *Ind. Eng. Chem. Res.* 2018, 57, 10269–1028
- 19)** Siddiqi, G.; Sun, P. P.; Galvita, V.; Bell, Catalyst performance of novel Pt/Mg(Ga)(Al)O catalysts for alkane dehydrogenation, *J. Catal.* 2010, 274, 200–206.
- 20)** Sun, P. P.; Siddiqi, G.; Chi, M. F.; Bell, Synthesis and characterization of a new catalyst Pt/Mg(Ga)(Al)O for alkane dehydrogenation, *J. Catal.* 2010, 274, 192–199.
- 21)** Horiuti, J.; Polanyi, M. *Trans. Faraday Soc.* 1934, 30, 1164.
- 22)** Galvita, V.; Siddiqi, G.; Sun, P. P.; Bell, A. T. Ethane dehydrogenation on Pt/Mg(Al)O and PtSn/Mg(Al)O catalysts, *J. Catal.* 2010, 271, 209–219.
- 23)** Li, Q.; Sui, Z. J.; Zhou, X. G.; Chen, D., Effect of air addition on the catalytic performance of Pt-Sn/Al₂O₃ catalysts in propane dehydrogenation, *Appl. Catal., A* 2011, 398, 18–26.
- 24)** Zhu, J.; Yang, M. L.; Yu, Y. D.; Zhu, Y. A.; Sui, Z. J.; Zhou, X. G.; Holmen, A.; Chen, D. *ACS Catal.* 2015, 5, 6310–6319.
- 25)** Zhao, Z. J.; Chiu, C. C.; Gong, J. L., Molecular understandings on the activation of light hydrocarbons over heterogeneous catalysts, *Chem. Sci.* 2015, 6, 4403–4425.
- 26)** Zhu, J.; Yang, M. L.; Yu, Y. D.; Zhu, Y. A.; Sui, Z. J.; Zhou, X. G.; Holmen, A.; Chen, D. *ACS Catal.* 2015, 5, 6310–6319.

- 27)** Valcárcel, A.; Ricart, J. M.; Clotet, A.; Illas, F.; Markovits, A.; Minot, C., A Theoretical Study of Catalytic Coupling of Propyne on Cu{111}, *J. Catal.* 2006, 241, 115–122.
- 28)** Chen, Y.; Vlachos, D. G., Hydrogenation of Ethylene and Dehydrogenation and Hydrogenolysis of Ethane on Pt(111) and Pt(211): A Density Functional Theory Study, *J. Phys. Chem. C* 2010, 114, 4973–4982.
- 29)** Boudart, M., Turnover Rates in Heterogeneous Catalysis, *Chem. Rev.* 1995, 95, 661–666.
- 30)** Larsson, M.; Hultén, M.; Blekkan, E. A.; Andersson, B. *J. Catal.* 1996, 164, 44–53.
- 31)** Borodziński, A.; Cybulski, A. The Kinetic Model of Hydrogenation of Acetylene-Ethylene Mixtures over Palladium Surface Covered by Carbonaceous Deposits. *Appl. Catal., A* 2000, 198, 51–66.
- 32)** Jarullah, A. T.; Mujtaba, I. M.; Wood, A. S. Kinetic Model Development and Simulation of Simultaneous Hydrodenitrogenation and Hydrodemetallization of Crude Oil in Trickle Bed Reactor. *Fuel* 2011, 90, 2165–2181.
- 33)** Tirado, A.; Ancheyta, J.; Trejo, F. Kinetic and Reactor Modeling of Catalytic Hydrotreatment of Vegetable Oils. *Energy Fuels* 2018, 32, 7245–7261.
- (34)** Roininen, J.; Alopaeus, V.; Toppinen, S.; Aittamaa, J. Modeling and Simulation of an Industrial Trickle-Bed Reactor for Benzene Hydrogenation: Model Validation against Plant Data. *Ind. Eng. Chem. Res.* 2009, 48, 1866–1872.
- (35)** Caputo, T.; Lisi, L.; Pirone, R.; Russo, G. Kinetics of the Preferential Oxidation of CO over CuO/CeO₂ Catalysts in H₂-Rich Gases. *Ind. Eng. Chem. Res.* 2007, 46, 6793–6800.
- (36)** Toppinen, S.; Rantakylä, T. K.; Salmi, T.; Aittamaa, J. Kinetics of the Liquid-Phase Hydrogenation of Benzene and Some Monosubstituted Alkylbenzenes over a Nickel Catalyst. *Ind. Eng. Chem. Res.* 1996, 35, 1824–1833
- (37)** Aghalayam, P.; Park, Y. K.; Vlachos, D. G. Construction and Optimization of Complex Surface-Reaction Mechanisms. *AIChE J.* 2000, 46, 2017–2029.
- (38)** Ulissi, Z. W.; Medford, A. J.; Bligaard, T.; Nørskov, J. K. To Address Surface Reaction Network Complexity Using Scaling Relations Machine Learning and DFT Calculations. *Nat. Commun.* 2017, 8, 1–7.

- (39) Fooshee, D.; Mood, A.; Gutman, E.; Tavakoli, M.; Urban, G.; Liu, F.; Huynh, N.; Van Vranken, D.; Baldi, P. Deep Learning for Chemical Reaction Prediction. *Mol. Syst. Des. Eng.* 2018, 3, 442–452.
- (40) Broadbelt, L. J.; Stark, S. M.; Klein, M. T. Computer Generated Pyrolysis Modeling: On-the-Fly Generation of Species, Reactions, and Rates. *Ind. Eng. Chem. Res.* 1994, 33, 790–799.
- (41) Valdés-Perez, R. E.; Zeigarnik, A. V. Interactive Elucidation (without Programming) of Reaction Mechanisms in Heterogeneous Catalysis. *J. Mol. Catal. A: Chem.* 1997, 119, 405–414.
- (42) Rangarajan, S.; Bhan, A.; Daoutidis, P. Language-Oriented Rule- Based Reaction Network Generation and Analysis: Description of RING. *Comput. Chem. Eng.* 2012, 45, 114–123.
- (43) Goldsmith, C. F.; West, R. H. Automatic Generation of Microkinetic Mechanisms for Heterogeneous Catalysis. *J. Phys. Chem. C* 2017, 121, 9970–9981.
- (44) Broadbelt, L. J.; Stark, S. M.; Klein, M. T. Termination of Computer-Generated Reaction Mechanisms: Species Rank-Based Convergence Criterion. *Ind. Eng. Chem. Res.* 1995, 34, 2566–2573.
- (45) Klinke, D. J.; Broadbelt, L. J. Mechanism Reduction during Computer Generation of Compact Reaction Models. *AIChE J.* 1997, 43, 1828–1837.
- (46) R. J. Koestner, J. C. Frost, P. C. Stair, M. A. V. Hove and G. A. Somorjai, Chemisorption of C3 hydrocarbons on cobalt silica-supported Fischer–Tropsch catalysts, *Surf. Sci.*, 1982, 116, 85.
- (47) Lee and F. Zaera, Thermal Chemistry of C4 Hydrocarbons on Pt(111): Mechanism for Double-Bond Isomerization, *J. Phys. Chem. B*, 109(7), 2745-2753 (2005).

Appendix 1. Athena Visual Studio code to solve DAE system as defined in section 4.2.2

! Microkinetic and reactor model simulation based on reaction scheme proposed in this work for PDH based on Pt catalyst.

! k_i 's represent forward rate constant, j_i 's represent equilibrium rate constant and K_a, K_d & K_e are the equilibrium constants for alkane adsorption/desorption reactions.

! R is the gas constant in $\text{mol}^3\text{bar/mol.K}$, T is temperature in kelvin, v is the total volumetric flow rate in m^3/sec

!=====

Global

$k_1, j_1, k_2, j_2, k_3, j_3, k_4, j_4, k_5, j_5, k_6, j_6, k_7, j_7, k_8, j_8, k_9, j_9, k_{10}, j_{10}, k_{11}, j_{11}, k_{12}, j_{12}, k_{13}, j_{13}, k_{14}, j_{14}, k_{15}, j_{15}, k_{16}, j_{16}, k_{17}, j_{17}, k_{18}, j_{18}, k_{19}, j_{19}, k_{20}, k_{21}, j_{21}, k_{22}, j_{22}, k_{23}, j_{23}, k_b, j_b, k_c, j_c, k_f, j_f, K_a, K_d, K_e, R, T, v, C$ As Real

$k_1 = 9.2\text{E}+6$

$j_1 = 3.1\text{E}-2$

$k_2 = 8.4\text{E}06$

$j_2 = 2.6\text{E}-2$

$k_3 = 1.3\text{E}+8$

$j_3 = 2.8\text{E}-01$

$k_4 = 7.5\text{E}+8$

$j_4 = 1.7$

$k_5 = 6.0\text{E}+7$

$j_5 = 3.5\text{E}-1$

$k_6 = 7.0\text{E}+8$

$j_6 = 2.1$

$k_7 = 2.2\text{E}+8$

$j_7 = 6.5\text{E}-1$

$k_8 = 7.6\text{E}+8$

$j_8 = 6.2$

$$k9 = 6.4E+8$$

$$j9 = 4.1$$

$$k10 = 1.4E+9$$

$$j10 = 3.7E+1$$

$$k11 = 1.2E+9$$

$$j11 = 36$$

$$k12 = 2.2E+8$$

$$j12 = 3.8$$

$$k13 = 1.0E+7$$

$$j13 = 6.7E+3$$

$$k14 = 5.1E+2$$

$$j14 = 7.6E-06$$

$$k15 = 1.2E+08$$

$$j15 = 1.1E-1$$

$$k16 = 1.9E+11$$

$$j16 = 1.4E+3$$

$$k17 = 1.4E+6$$

$$j17 = 3.2E-3$$

$$k18 = 9.4E8$$

$$j18 = 2.6$$

$$k19 = 1.6E+11$$

$$j19 = 2.6E+4$$

$$k20 = 3.1E+3$$

$$k21 = 1.5E+9$$

$$j21 = 2.8E+4$$

$$k22 = 3.1E+9$$

$$j22 = 1.3E+3$$

$$k23 = 4.8E+9$$

$$j23 = 38$$

$$k_b = 1.4E+8$$

$$j_b = 4.6E-04$$

$$k_c = 2.0E+8$$

$$j_c = 8.1E-1$$

$$k_f = 1.7E+8$$

$$j_f = 2.0E-02$$

$$K_a = 3.9E-03$$

$$K_d = 1$$

$$K_e = 2.7E-02$$

$$R = 8.314E-5$$

$$\text{Temp} = 873$$

$$v = 10E-6$$

$$C = R * \text{Temp} / v$$

@Initial Conditions

$$U(1) = 8.06E-06 \quad ! \text{C}_3\text{H}_8(\text{g})$$

$$U(2) = 0 \quad ! \text{C}_3\text{H}_6(\text{g})$$

$$U(3) = 0 \quad ! \text{CH}_4(\text{g})$$

$$U(4) = 1.03E-05 \quad ! \text{H}_2(\text{g})$$

$$U(5) = 0 \quad ! \text{C}_2\text{H}_6(\text{g})$$

$$U(6) = 0 \quad ! \text{C}_2\text{H}_4(\text{g})$$

$$U(7) = 0 \quad ! \text{Byproduct from reaction no. 20}$$

$$U(8) = 0 \quad ! \text{H}^*$$

$$U(9) = 0 \quad ! \text{1-propyl}$$

$$U(10) = 0 \quad ! \text{2-propyl}$$

$$U(11) = 0 \quad ! \text{1-propylidene}$$

$$U(12) = 0 \quad ! \text{2-propylidene}$$

$$U(13) = 0 \quad ! \text{propylene}$$

$$U(14) = 0 \quad ! \text{1-propenyl}$$

U(15) = 0 ! 2-propenyl
 U(16) = 0 ! propyne
 U(17) = 0 ! ethylidyne
 U(18) = 0 ! methylidyne
 U(19) = 0 ! atomic c
 U(20) = 0 ! methyl
 U(21) = 0 ! methylidene
 U(22) = 0 ! ethyl
 U(23) = 0 ! ethylidene
 U(24) = 0 ! ethylene
 U(25) = 1 ! surface vacancy/free sites
 U(26) = 0 ! %Conversion
 U(27) = 0 ! %selectivity of C3H6(g)
 U(28) = 0 ! %selectivity of CH4(g)
 U(29) = 0 ! %selectivity of C2H6(g)
 U(30) = 0 ! %selectivity of C2H4(g)

@Coefficient Matrix

E(1) = 1.0
 E(2) = 1.0
 E(3) = 1.0
 E(4) = 1.0
 E(5) = 1.0
 E(6) = 1.0
 E(7) = 1.0

! ri's are the rate expressions for all surface and adsorption/desorption reactions

@Model Equations

Dim r1,r2,r3,r4,r5,r6,r7,r8,r9,r10,r11,r12,r13,r14,r15,r16,r17,r18,r19,r20,r21,r22,r23,rb,rc,rf As Real

r1 = k1*(Ka*U(25)^2*C*U(1) - (U(8)*U(9)/j1))

$$r2 = k2*(Ka*U(25)^2*C*U(1) - (U(8)*U(10)/j2))$$

$$r3 = k3*(U(25)*U(9) - (U(11)*U(8)/j3))$$

$$r4 = k4*(U(25)*U(9) - (U(13)*U(8)/j4))$$

$$r5 = k5*(U(25)*U(10) - (U(12)*U(8)/j5))$$

$$r6 = k6*(U(25)*U(10) - (U(13)*U(8)/j6))$$

$$r7 = k7*(U(25)*U(13) - (U(14)*U(8)/j7))$$

$$r8 = k8*(U(25)*U(13) - (U(15)*U(8)/j8))$$

$$r9 = k9*(U(25)*U(11) - (U(14)*U(8)/j9))$$

$$r10 = k10*(U(25)*U(12) - (U(15)*U(8)/j10))$$

$$r11 = k11*(U(25)*U(14) - (U(16)*U(8)/j11))$$

$$r12 = k12*(U(25)*U(15) - (U(16)*U(8)/j12))$$

$$r13 = k13*(U(25)*U(16) - (U(17)*U(8)/j13))$$

$$r14 = k14*(U(25)*U(17) - (U(20)*U(8)/j14))$$

$$r15 = k15*(U(25)*U(20) - (U(21)*U(8)/j15))$$

$$r16 = k16*(U(25)*U(21) - (U(18)*U(8)/j16))$$

$$r17 = k17*(U(25)*U(18) - (U(19)*U(8)/j17))$$

$$r18 = k18*(U(25)*U(22) - (U(23)*U(8)/j18))$$

$$r19 = k19*(U(25)*U(23) - (U(17)*U(8)/j19))$$

$$r20 = k20*U(19)$$

$$r21 = k21*(U(20)*U(8) - (Kd*C*U(3)*U(25)^2/j21))$$

$$r22 = k22*(U(22)*U(8) - (Ke*C*U(5)*U(25)^2/j22))$$

$$r23 = k23*(U(22)*U(25) - (U(24)*U(8)/j23))$$

$$rb = kb*(C*U(2)*U(25) - U(13)/jb)$$

$$rc = kc*(C*U(4)*U(25)^2 - (U(8)^2)/jc)$$

$$rf = kf*(C*U(6)*U(25) - U(24)/jf)$$

! 3E-05 is the factor that is multiplied by each rate expression to make units right.

$$F(01) = (-r1-r2)*3E-05$$

$$F(02) = -rb*3E-05$$

$$F(03) = r21*3E-05$$

$$F(04) = -rc*3E-05$$

$$F(05) = r22*3E-05$$

$$F(06) = -rf*3E-05$$

$$F(07) = r20*3E-05$$

$$F(08) = (r1+r2+r3+r4+r5+r6+r7+r8+r9+r10+r11+r12+r15+r16+r17+r18+r19-r21-r22+r23+2*rc)*3E-05$$

$$F(09) = (r1 - r3 - r4)*3E-05$$

$$F(10) = (r2 - r5 - r6)*3E-05$$

$$F(11) = (r3 - r9)*3E-05$$

$$F(12) = (r5 - r10)*3E-05$$

$$F(13) = (r4 + r6 - r7 - r8 + rb)*3E-05$$

$$F(14) = (r7 + r9 - r11)*3E-05$$

$$F(15) = (r8 + r10 - r12)*3E-05$$

$$F(16) = (r11 + r12 - r13)*3E-05$$

$$F(17) = (r13 - r14 + r19)*3E-05$$

$$F(18) = (r13 - r17 + r16)*3E-05$$

$$F(19) = (r14 + r17 - r20)*3E-05$$

$$F(20) = (r14 - r15 - r21)*3E-05$$

$$F(21) = (r15 - r16)*3E-05$$

$$F(22) = (-r18 - r22 - r23)*3E-05$$

$$F(23) = (r18 - r19)*3E-05$$

$$F(24) = (r23 + rf)*3E-05$$

$$F(25) = (1 - U(8)- U(9)- U(10)- U(11)- U(12)- U(13)- U(14)- U(15)- U(16)- U(17)- U(18)- U(19)- U(20)- U(21)- U(22)- U(23)- U(24)- U(25))/(1 + Ka*C*U(1) + Kd*C*U(3)+ Ke*C*U(5))$$

$$F(26) = U(26) - (8.06E-06 - U(1))*100/8.06E-06$$

$$F(27) = U(27)*(8.061E-06 - U(1)) - (U(2)*100)$$

$$F(28) = U(28) - (U(3)*100)/(3*(8.061E-06 - U(1)))$$

$$F(29) = U(29) - (U(5)*200)/(3*(8.061E-06 - U(1)))$$

$$F(30) = U(30) - (U(6)*200)/(3*(8.061E-06 - U(1)))$$

CHAPTER 2

This chapter is dedicated to the work that has been carried out along with the main work of microkinetic modeling of PDH. The motive behind this exercise is to understand the concept of parameter estimation in reaction kinetics, which can be used further in adjusting the parameters of a microkinetic model following the experimental data available.

1. Problem statement

The problem is to estimate the kinetic rate constants (k_1 - k_9) as parameters for a given set of reaction scheme proposed by Van Damme et al.^[1] with minimal cross-correlation. Figure 1 below shows the reaction scheme along with the respective rate laws. As stated in the literature^[1], such a molecular scheme is an approximation of the real radical scheme.

Reaction	Rate equation
1. $C_3H_8 \xrightarrow{k1} C_2H_4 + CH_4$	$r1 = k1 * C_{C_3H_8}$
2. $C_3H_8 \xrightleftharpoons[k2]{K2} C_3H_6 + H_2$	$r2 = k2 * \left(C_{C_3H_8} - \frac{C_{C_3H_6} * C_{H_2}}{K_2} \right)$
3. $C_3H_8 + C_2H_4 \xrightarrow{k3} C_2H_6 + C_3H_6$	$r3 = k3 * C_{C_3H_8} * C_{C_2H_4}$
4. $2C_3H_6 \xrightarrow{k4} 3C_2H_4$	$r4 = k4 * C_{C_3H_6}$
5. $2C_3H_6 \xrightarrow{k5} 0.5C_6 + 3CH_4$	$r5 = k5 * C_{C_3H_6}$
6. $C_3H_6 \xrightleftharpoons[k6]{K6} C_2H_2 + CH_4$	$r6 = k6 * \left(C_{C_3H_6} - \frac{C_{C_2H_2} * C_{CH_4}}{K_6} \right)$
7. $C_3H_6 + C_2H_6 \xrightarrow{k7} C_4H_8 + CH_4$	$r7 = k7 * C_{C_3H_6} * C_{C_2H_6}$
8. $C_2H_6 \xrightleftharpoons[k8]{K8} C_2H_4 + H_2$	$r8 = k8 * \left(C_{C_2H_6} - \frac{C_{C_2H_4} * C_{H_2}}{K_8} \right)$
9. $C_2H_4 + C_2H_2 \xrightarrow{k9} C_4H_6$	$r9 = k9 * C_{C_2H_4} * C_{C_2H_2}$

Figure 1: Molecular Reaction scheme for thermal cracking of propane

In the proposed reaction scheme, 9 reactions (6 irreversible & 3 reversible) contain 10 species (each species has a representation number according to Table 1 in Appendix-A).

2. Modeling of reactions

Formulation of rate laws

To write the reaction rates for any reaction, the approach we followed has been adapted from the article authored by Sundaram and Froment.^[2] Formulated reaction rates are given in figure 2. Assumptions while formulating these rates are as follows:

- 1) Gases are assumed to be ideal, as evident from the rate laws $\{C = \frac{n}{V} = \frac{P}{RT}\}$
- 2) The molar fraction is assumed to be equal to the volume fraction. This is evident from the term F_j/F_t (volume fraction) in the rate laws, used in place of mole fraction.

The reaction of thermal cracking was carried out in an isothermal tubular reactor with plug flow. The mass balance on propane over an isothermal differential volume element for such a case may be written as

$$\frac{dF_j}{dV_r} = R_j = \sum \alpha_{ij} r_i \quad (1)$$

V_r is the equivalent reactor volume

α_{ij} is the stoichiometric coefficient of the j th component in the i th reaction

Mass balance over each species is applied according to equation (1) to result in 10 Coupled ordinary differential equations (as shown in figure 2) containing 12 unknown parameters ($k_1 - k_9$, K_2 , K_6 , K_8). Initially, the focus is to determine only 9 parameters ($k_1 - k_9$), taking equilibrium constants values from the Sundaram and Froment at 800 °C.^[2] (values are given in Table 2 Appendix-A)

To eliminate the influence of the temperature profile, the space time is based on the equivalent reactor volume V_r . The equivalent reactor volume V_r is defined as that volume which, at a reference temperature T_R and a reference total pressure P_R , would give the same conversion as the actual reactor volume, with its temperature and pressure profiles.^[1]

3. Data Collection

The data regarding the flow rates for the species involved in the reaction scheme were obtained from various graphs provided in the article by Van Damme *et al.* The data points for the species were given as yield weight % vs. conversion of propane. The volume of the reactor (V_r) required for the parameter estimation was extracted from the plots shown in the same article as V/F_0 vs. conversion of propane. All the data points needed were collected at the reaction temperature 800 °C for class 3 type of reaction conditions (Table 3 in Appendix A) using an online tool called “webplotdigitizer” and are tabulated in Appendix 1.

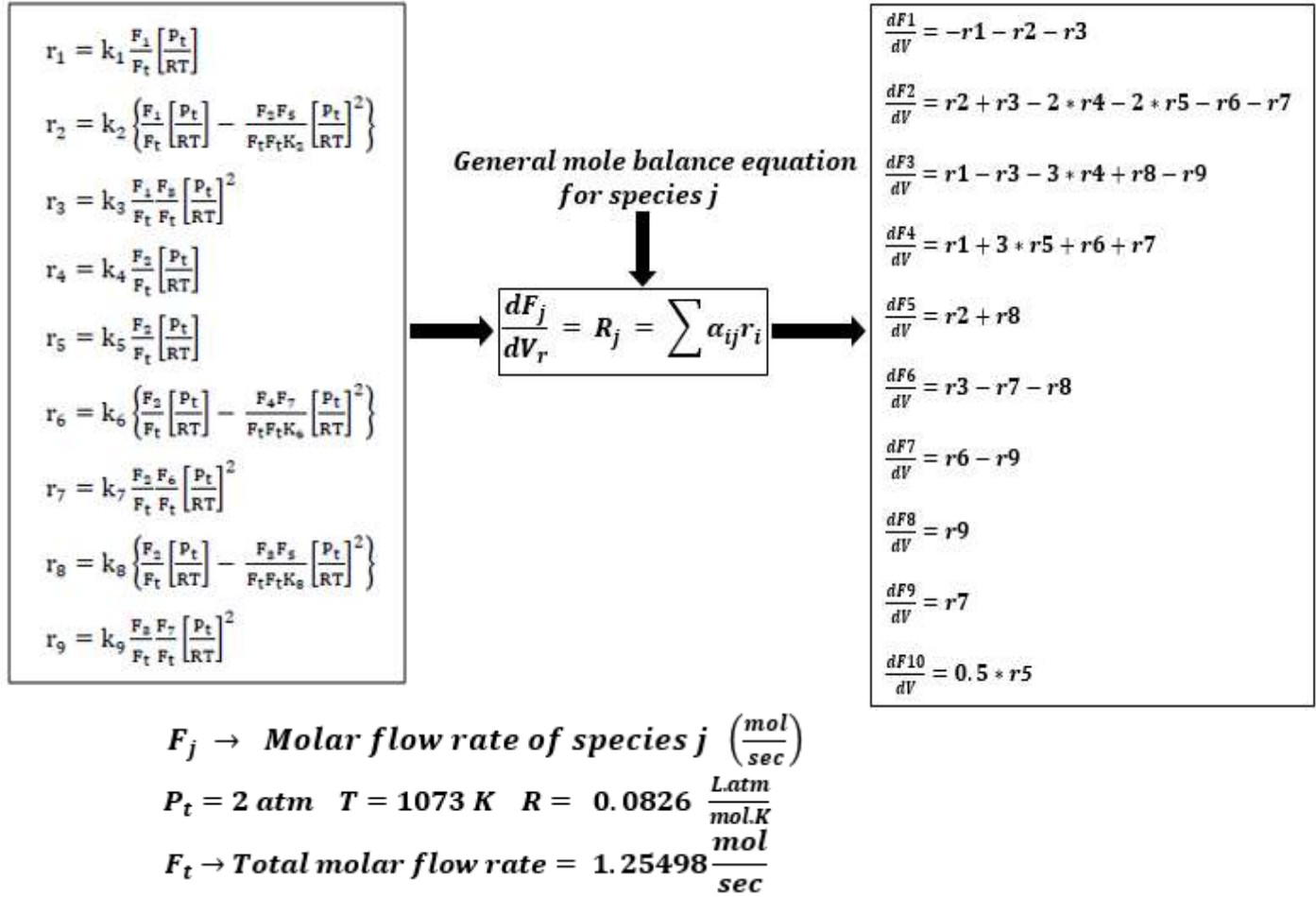


Figure 2: Formulated rate laws and mass balance equation for all species.

4. Selection of basis and calculation of initial feed composition

- To estimate the parameters and get relevant data, a basis is necessary to ease the work. Data for various products were available in the form of yield wt. %, defined as kilogram of product/100 kilogram of propane fed. Hence, to find out product yields, the basis was chosen as 100 kg/hour of a propane feed. Conversion of the propane feed from kg/hour to moles/s is shown below

$$100 \frac{\text{kg}}{\text{hr}} \text{ propane} = \frac{100 * 1000}{3600} \frac{\text{g}}{\text{s}} = \frac{100 * 1000}{3600 * 44} \frac{\text{moles}}{\text{s}} = 0.6313 \frac{\text{moles}}{\text{s}} \text{ of propane fed}(F_0)$$

F_0 is the basis for the rest of the calculation in this work.

- The molar flow rate of steam fed as a diluent is calculated based on the steam dilution factor used for the class 3 experiment and found to be 0.6173 moles/s.

- A significant part of the feed (without steam) is propane. But few other compounds are also present. A range of values as feed is given in Van Damme *et al.*,^[1] out of which the feed ratio was fixed to solve for the current problem as the first estimate for parameters (i.e., rate constants) and to estimate total molar flow rate (F_t), results are tabulated in Table 4 Appendix-A
- The rate laws for the propane cracking reaction scheme have been written in terms of the molar flow rate of the species, so to obtain these flow rates, we use the given data of yield wt % vs. conversion and V/F_0 vs. conversion (X_p). The data conversion is carried out by utilizing the formula we had developed, given in Appendix-B.

Finally, we had 17 data points for equivalent reactor volume (V_r), and corresponding to each V_r point, we got the molar flow rate (F_j) for all 10 species. All data points are shown in Table 5 Appendix-C.

5. Parameter estimation Using Athena Visual Studio and Python Lmfit package: Methodology

In Athena visual studio, various inputs were given in order to estimate all the parameters (k_1 - k_9) in the Parameter estimation solver control panel. We had used both Bayesian estimation and the Non-linear least-square approaches, which resulted in the same set of parameters. Initial guesses for parameters were given from Van Damme et al. paper.

In the python lmfit package, we have estimated all parameters in a Non-linear least-square manner, taking an objective function as the sum of the square of residual (residual = model prediction – data) over all data points. Minimization of this objective function was achieved through the Levenberg-Marquardt algorithm. Python inbuilt ode solver was used to solve coupled ode system to result in model prediction. Initial guesses for parameters were given both from Van Damme et al. and parameters estimated from Athena visual studio.

6. Results and Discussion

1) All the parameters were estimated in Athena and Python, which are shown in Figure 3. Athena resulted in a set of parameters that were way different in order of magnitude as compared to Van Damme et al. k 's. On the other hand, the L-M algorithm couldn't converge the solution when initial guesses were given from Van damme et al. However, it resulted in the same set of parameters (in terms of the order of magnitude) when Athena's solution was given as an initial guess.


2) To check the correctness of numerical modeling of reactions, we have digitalized the Van Damme et al. model predictions^[3] given in terms of yield wt % vs. Propane conversion % for four major species (C_3H_6 , C_2H_4 , CH_4 , H_2). Using our numerical solver for coupled ode, we have

overlapped our results (dotted lines) over Van Damme et al. predictions (solid lines) by taking two cases as follows:

Case 1: Coupled ODE's were first solved for parameter values, given in the Van Damme et al. (Figure 4A).

Case 2: Coupled ODE's were solved for parameter values, estimated in Athena Visual Studio (Figure 4B).

Ideally, we should get the complete overlapping of Van Damme et al. model predictions (solid lines) and our model predictions (dotted lines) in Figure 4(A). Still, there are small deviations for all species, and the reason behind it can be F_t 's value, which varies from 1.2518 to 1.8 mol/s.



Rate Constants	Van Damme k's	Athena k's	L-M Algorithm(Python)
k1	2.341	8.8781E-04	8.8885E-04
k2 ⁺	2.12	8.1509E-04	8.5371E-04
k3	23.635	7.3903E-02	5.7110E-02
k4	0.721	5.9872E-04	4.2747E-04
k5 ⁺	0.816	2.2684E-04	3.8179E-04
k6	0.305	1.5042E-04	1.7608E-04
k7 ⁺	334.2	3.0121E-01	8.2637E-02
k8	2.416	3.9034E-04	3.7740E-04
k9	4064	2.6318E+00	1.3808E+00

Unit: sec^{-1} or $+ \text{L mol}^{-1} \text{sec}^{-1}$

Figure 3: Rate constant values from Van Damme et al. and estimated rate constants from Athena Visual Studio and Python Lmfit package (Using L-M algorithm)

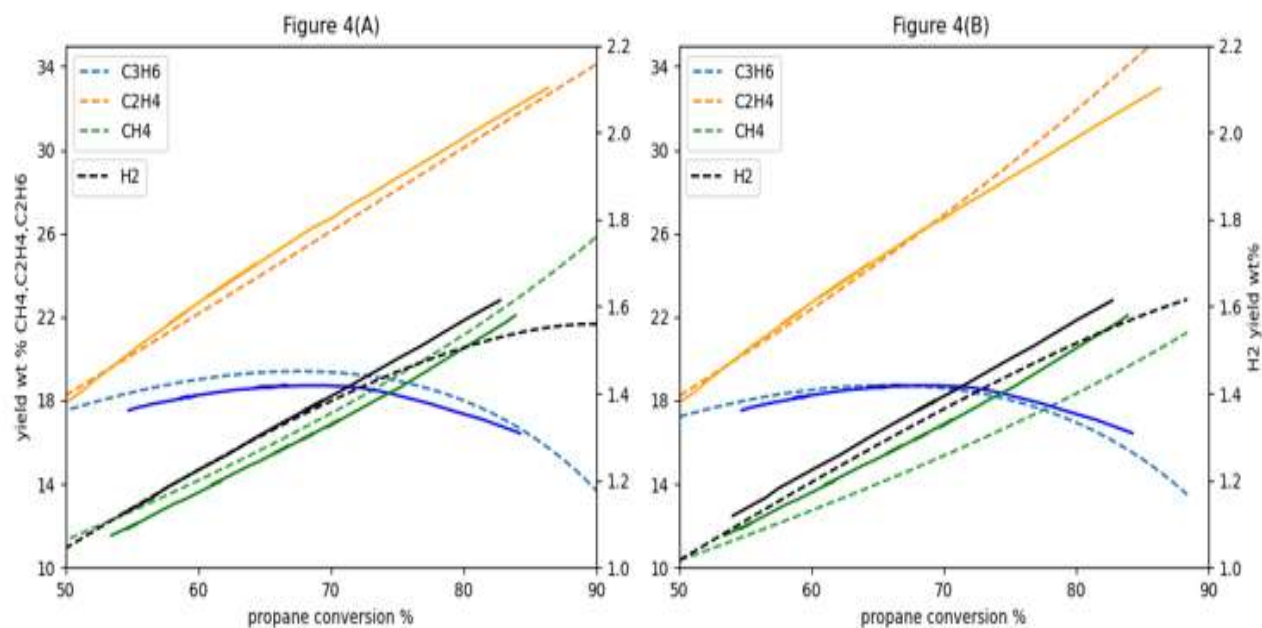


Figure 4: Solid lines represent model prediction by Van Damme et al., and dotted line represent model prediction using k 's value from (A) Van Damme et al. (B) Athena's

3) Even though there are small residuals (predicted value – observed value) for almost all species (Appendix D) for Athena's and Python's estimated rate constants, but large off-diagonal elements in the correlation matrix (Figure 5) indicates that there are high correlations among different pairs of rate constants.

	k1	k2	k3	k4	k5	k6	k7	k8	k9
k1	1								
k2	0.277	1							
k3	-0.258	-0.502	1						
k4	-0.354	-0.179	0.697	1					
k5	0.048	0.023	-0.071	-0.180	1				
k6	0.029	-0.006	-0.074	0.043	0.107	1			
k7	0.019	0.092	-0.280	-0.390	0.042	0.011	1		
k8	-0.430	0.501	-0.530	-0.237	0.035	0.005	0.169	1	
k9	-0.063	-0.053	0.035	0.031	-0.020	-0.644	-0.006	0.002	1

Figure 5: Parameter Correlation matrix

4) An approximate calculation of rate constant k_1 is performed for the initial 5% conversion, assuming that there is only propane in the feed initially as follows:

$$\begin{array}{lcl}
 C_3H_8 & \xrightarrow{k_1} & C_2H_4 + CH_4 \\
 \frac{dF}{dV} = k_1 * C = k_1 * \frac{P}{RT} & & T = 1073K, P = 2atm, R = 0.0826 \frac{L \cdot atm}{mol \cdot K} \\
 \frac{dF}{dV} = \frac{(0.6313 - 0.599735)}{(1516.18 - 0)} = 2.08e-05 \frac{mol}{l \cdot s} & & C = \frac{P}{RT} = 0.02257 \frac{mol}{l} \\
 \boxed{k_1 = \frac{2.08e-05}{0.02257} = 9.23e-04 s^{-1}} & &
 \end{array}$$

The above estimated k_1 is of the same order of magnitude as estimated in Athena and Python.

References:

- 1) P. S. Van Damme, S. Narayanan, and G. F. Froment, "Thermal Cracking of Propane and Propane-Propylene Mixture: Pilot Plant Versus Industrial Data," American Institute of Chemical Engineering, vol. 21, no. 6, pp. 1065–1073, 1975.
- 2) K. M. Sundaram and G. F. Froment, "Modeling of Thermal Cracking Kinetics-I; Thermal Cracking of Ethane Propane and Their Mixtures," Chemical Engineering Sciences, vol. 32, no. 3, pp. 601–608, 1977.
- 3) Chemical Reactor Analysis and Design by Gilbert F. Froment & Kenneth B. Bischoff, Chapter 1, Example 1.6.2-3 Thermal Cracking of Propane, Page No.57.

Appendix-A

Table 1: Species and symbolic numerals (j)

Compound	j	Molecular Weight (g/mol)
Propane (C ₃ H ₈)	1	44
Propylene (C ₃ H ₆)	2	42
Ethylene (C ₂ H ₄)	3	28
Methane (CH ₄)	4	16
Hydrogen (H ₂)	5	2
Ethane (C ₂ H ₆)	6	30
Acetylene (C ₂ H ₂)	7	26
Butyne (C ₄ H ₆)	8	54
Butene (C ₄ H ₈)	9	56
C ₆	10	72

Table 2: Equilibrium rate constants ^[2] values at T = 800 °C

K2	0.102
K6	0.01375
K8	0.01276

Table 3: Classification of experiments

Class	Total outlet pressure (atm. abs.)	Steam dilution (kg of steam/kg of propane)	Total inlet pressure (atm. abs.)
1	1.4	0.4	0.75
2	1.4	1.0	0.45
3	2.0	0.4	1.2
4	2.0	1.0	0.65

Table 4: Initial Molar flow rate in the feed

Species	Molar flow rate (mole/s)
C ₃ H ₈	0.6313
C ₃ H ₆	0.0027
C ₂ H ₆	0.0004
> C ₃	0.0001

Total feed molar flow rate, F_t then comes out to be equal to, $F_t = 0.6313 + 0.6173 + 0.0027 + 0.0004 + 0.0001 = 1.2518$ mole/s

Appendix-B Formulas to convert data of yield wt. % vs. conversion and V/F₀ vs. conversion (X_p) to Molar flow rate vs. V_e

1) Changing the volume units to liter from m³ and converting V/F₀ data to V_r using below given formula

$$V_E(l) = \frac{V}{F_0} * 1000 * F_0$$

2) To convert yield wt% data for the jth compound to F_j. The following calculation is done. Let y be the magnitude of yield wt% for any jth component at any conversion %. Then

$$F_j \left(\frac{\text{moles}}{s} \right) = \frac{y * 44 * F_0}{MW_j} = \frac{y * 44 * 0.6316}{MW_j}$$

Where MW_j is the molecular weight of the jth species.

3) For Propane, the molar flow rate was calculated using the conversion formula

$$F_1 \left(\frac{\text{moles}}{s} \right) = \frac{(100 - X_p) * F_0}{100}$$

Appendix-C

Table 5: Molar flow rate of the j^{th} species (mole/s) and the effective reactor volume (L)

V(l)	C3H8	C3H6	C2H4	CH4	H2	C2H6	C2H2	C4H6	C4H8	C6
0	0.6313	0.002713	0.001	0.001	0.001	0.00044	0.00001	0.00005	0.00001	0.00007
1588.997	0.599327	0.017858	0.012464	0.01138	0.01449	0.00088	3.21E-06	0	2.37E-05	0
3263.229	0.56783	0.033959	0.027185	0.025313	0.02941	0.002742	4.27E-06	0	0.000131	0
5074.132	0.536266	0.047208	0.043719	0.041168	0.043043	0.004639	5.34E-06	0	0.000433	7.32E-05
6953.371	0.504707	0.060677	0.059797	0.060225	0.057102	0.007394	1.71E-05	5.18E-05	0.000483	8.60E-05
8832.611	0.473101	0.072171	0.076326	0.079923	0.072027	0.010574	2.86E-05	0.000193	0.000857	0.000448
10917.6	0.4415	0.083885	0.093313	0.101542	0.086947	0.014181	4.36E-05	0.000512	0.001298	0.000728
13001.85	0.409857	0.093844	0.112104	0.122521	0.101437	0.017364	0.00012	0.000504	0.001789	0.001162
15222.77	0.378685	0.101608	0.131804	0.145421	0.115931	0.020116	0.000196	0.000987	0.002264	0.001706
17580.36	0.346954	0.107838	0.151952	0.168971	0.130421	0.023296	0.000273	0.00162	0.002738	0.002328
20143.7	0.315192	0.112752	0.172104	0.195074	0.145776	0.026051	0.000413	0.00244	0.003163	0.002987
22911.31	0.283932	0.116788	0.192705	0.219255	0.159835	0.028804	0.000617	0.003373	0.003537	0.003873
26498.95	0.252118	0.119508	0.213757	0.245999	0.17476	0.031128	0.000948	0.004381	0.003778	0.005026
31180.7	0.220795	0.120912	0.235718	0.276594	0.18925	0.034308	0.001343	0.005521	0.003953	0.006633
36886.76	0.188909	0.120562	0.257675	0.30654	0.20417	0.036208	0.001897	0.006773	0.003978	0.00877
44301.95	0.157497	0.118236	0.280089	0.337767	0.219095	0.038532	0.002515	0.008006	0.003853	0.011324
53698.89	0.126014	0.112839	0.303859	0.370284	0.232723	0.039574	0.003324	0.009409	0.003529	0.01494

Appendix-D Residual vs. event number graphs for all species

